

November 2019

Phasor Measurement Unit Data-Based Steady State and Dynamic Model Estimation

Anas Almunif
University of South Florida

Follow this and additional works at: <https://scholarcommons.usf.edu/etd>

 Part of the [Engineering Commons](#)

Scholar Commons Citation

Almunif, Anas, "Phasor Measurement Unit Data-Based Steady State and Dynamic Model Estimation" (2019). *Graduate Theses and Dissertations*.
<https://scholarcommons.usf.edu/etd/8001>

This Dissertation is brought to you for free and open access by the Graduate School at Scholar Commons. It has been accepted for inclusion in Graduate Theses and Dissertations by an authorized administrator of Scholar Commons. For more information, please contact scholarcommons@usf.edu.

Phasor Measurement Unit Data-Based Steady State and Dynamic Model Estimation

by

Anas Almunif

A dissertation submitted in partial fulfillment
of the requirements for the degree of
Doctor of Philosophy in Electrical Engineering
Department of Electrical Engineering
College of Engineering
University of South Florida

Major Professor: Lingling Fan, Ph.D.
Zhixin Miao, Ph.D.
Fangxing Li, Ph.D.
Qiong Zhang, Ph.D.
Yasin Yilmaz, Ph.D.

Date of Approval:
October 30, 2019

Keywords: PMU placement, observability, PMU measurements, eigenvalue identification,
power system oscillations

Copyright © 2019, Anas Almunif

Dedication

To my father and mother, to my brothers and sisters.

Acknowledgments

First and foremost, I would like to express my deepest gratitude and appreciation to my major advisor Dr. Lingling Fan for her support, guidance, and encouragement throughout the past few years. Dr. Fan was always available to discuss the research obstacles and provide helpful suggestions. I greatly appreciate her insightful comments and persistent help.

Second, I would like to thank Dr. Zhixin Miao for his help and support. I would also like to thank the committee members: Dr. Fangxing Li, Dr. Qiong Zhang, and Dr. Yasin Yilmaz for their helpful comments and suggestions.

I acknowledge with gratitude the full scholarship provided by Majmaah University and organized by Saudi Arabian Cultural Mission (SACM).

I would like to thank my recent colleagues from the Smart Grid Power Systems Laboratory, in particular Yin Li, Minyue Ma, Ibrahim Alsaleh, Miao Zhang, Abdullah Alassaf, Abdulhakim Alsaif, and my former colleagues Dr. Mohemmed Alhaider, Dr. Hossein G. Aghamolki, Dr. Ahmad Tazay, for the discussion and help.

Last but not least, I would like to specially thank my father, Prof. Abdulmohsen Almunif, and my mother, Sara Altuwaijri, for their continuous support and encouragement. My special thanks are extended to my brothers and sisters for their support.

Table of Contents

List of Tables	iii
List of Figures	iv
Abstract	vi
Chapter 1: Introduction	1
1.1 Background	1
1.2 Phasor Measurement Unit (PMU)	1
1.3 Optimal PMU Placement (OPP)	2
1.4 PMU for Inter-Area Oscillation Identification and Eigenvalue Estimation	3
1.5 Outline of the Dissertation	5
Chapter 2: Optimal PMU Placement for Steady State Estimation	6
2.1 Introduction	6
2.2 Mixed Integer Linear Programming	8
2.3 Nonlinear Programming	10
2.4 OPP Case Studies	14
2.4.1 Power Flow Measurements	14
2.4.1.1 MILP Approach	14
2.4.1.2 NLP Approach	15
2.4.1.3 Power Flow Measurement Example	15
2.4.2 Zero Injection Measurements	17
2.4.3 Limited Communication Facility	24
2.4.4 Single PMU Failure	25
2.4.5 Limited PMU Channel Capacity	26
2.4.6 Remarks on OPP Problem Simulation Results	28
2.5 Conclusion	31
Chapter 3: PMU Measurements for Oscillation Monitoring: Connecting Prony Analysis with Observability	32
3.1 Introduction	32
3.2 Prony Analysis	34
3.2.1 Prony Analysis Principle	34
3.2.2 Singular Value Decomposition of the Prony Analysis H Matrix	37

3.3	Modal Decomposition and Observability of Modes	37
3.4	Case Studies	39
3.4.1	Two-Area Four-Machine System	39
3.4.1.1	Comparison of Different Signals	39
3.4.1.2	Comparison of Model Order Assumption	41
3.4.2	16-Machine 68-Bus System	43
3.4.2.1	Sensitivity Analysis of Noise Level	46
3.5	Conclusion	47
Chapter 4: Measurement-Based Eigenvalue Identification Using Prony Analysis, Matrix Pencil and Eigensystem Realization Algorithm		48
4.1	Introduction	48
4.2	Principles of the Three Methods	52
4.2.1	Prony Analysis	52
4.2.2	Matrix Pencil	53
4.2.2.1	SVD-Based Rank Reduction	54
4.2.2.2	Multiple Channel Consideration	56
4.2.3	Eigensystem Realization Algorithm	57
4.3	Order Reduction Techniques	60
4.4	Case Studies	64
4.4.1	Large-Scale Power Grid Oscillations	64
4.4.2	Real-World Oscillation Events	66
4.4.2.1	Oscillation Event 1	67
4.4.2.2	Oscillation Event 2	68
4.4.3	Development Discussion	70
4.5	Conclusion	72
Chapter 5: Conclusion and Future Work		73
5.1	Conclusion	73
5.2	Future Work	74
5.2.1	Dynamic Parameter Estimation Background	74
5.2.2	Two-Machine Power System Model	76
5.2.3	Formulation of the Dynamic Parameter Estimation	79
5.2.4	Example	80
5.2.4.1	Sensitivity Analysis	81
References		83
Appendix A: MATLAB Code for Dynamic Parameter Estimation		92
Appendix B: Copyright Permissions		94
About the Author		End Page

List of Tables

Table 2.1	OPP results using MILP and NLP/SQP	14
Table 2.2	Power flow measurements case results	17
Table 2.3	Branches of power flow measurements	18
Table 2.4	Zero injection measurement locations	24
Table 2.5	Zero injection case results	24
Table 2.6	Limited communication facility case results	25
Table 2.7	Single PMU failure results	26
Table 2.8	Limited channel capacity case results	28
Table 2.9	MILP and NLP CPU time comparison	29
Table 2.10	Comparison results of zero injection using different methods	30
Table 2.11	OPP results for a large 2383-bus Polish system	30
Table 3.1	The observability approach of buses 1, 13, and 101 with damping ratio and frequency of the 13-bus system	40
Table 4.1	CPU time comparison of the three methods	72
Table 5.1	Two-machine model parameter estimation result	81
Table 5.2	Parameter estimation with different lower bound of T	82
Table 5.3	Parameter estimation with different lower bounds of D_1 and D_2	82

List of Figures

Figure 1.1	PMU locations in North American power grid.	2
Figure 1.2	Phasor measurement unit block diagram.	3
Figure 1.3	Phasor measurement unit installation cost.	4
Figure 2.1	IEEE 14-bus system.	13
Figure 2.2	Four-bus system.	18
Figure 2.3	Six-bus system.	19
Figure 3.1	The two-area four machine test case in PST.	40
Figure 3.2	Singular values for the Hankel matrices related to the six signals.	41
Figure 3.3	Comparison of the reconstructed signals against the original measurements (thin blue lines).	42
Figure 3.4	Singular values for the Hankel matrices related to three orders: 50, 120 and 220.	42
Figure 3.5	Comparison of the reconstructed signals against the original measurements for different model order assumptions.	43
Figure 3.6	16-machine, 68-bus test case.	43
Figure 3.7	Observability of different buses.	44
Figure 3.8	Oscillation modes 1 and 3 participation factor of the 68-bus system.	45

Figure 3.9	Singular values of the Hankel matrix corresponding to bus voltage measurement at 5, 29, and 67.	45
Figure 3.10	Comparison of the reconstructed signals against the original measurements.	46
Figure 3.11	Singular values of the Hankel matrix for different noise levels.	46
Figure 4.1	RLC circuit.	61
Figure 4.2	RLC circuit reconstructed signals and estimated eigenvalues with assumed order of 33.	62
Figure 4.3	RLC circuit reconstructed signals and estimated eigenvalues with assumed order of 3.	62
Figure 4.4	Reduced-order Prony analysis results of the RLC circuit.	63
Figure 4.5	Large-scale power grid oscillation signal reconstruction and eigenvalue estimation (Order is 10).	65
Figure 4.6	Large-scale power grid oscillation signal reconstruction and eigenvalue estimation (Order is 4).	67
Figure 4.7	Phase-to-ground voltage magnitudes during the oscillatory events.	69
Figure 4.8	Signal reconstruction and eigenvalue estimation of Event 1 with assumed order of 15.	69
Figure 4.9	Signal reconstruction and eigenvalue estimation of Event 1 with assumed order of 3.	70
Figure 4.10	Event 2 signal reconstruction and eigenvalue estimation.	71
Figure 5.1	Two-machine power system model.	76
Figure 5.2	Turbine model block diagram.	76

Abstract

Phasor measurement units (PMUs) have been put into power grid for real-time monitoring. This research investigates the PMU data for steady state estimation and dynamic model estimation. It focuses on three main research areas to enhance the security of the power system monitoring. First, optimal PMU placement (OPP) problem is developed to minimize the number of PMUs required for the system to be completely observable using mixed integer linear programming and nonlinear programming. Second, PMU measurements are ranked for oscillation monitoring based on two approaches: oscillation mode observability and Prony analysis. Further, the principles, multi-channel data handling, and noise resilience techniques of three eigenvalue identification methods used in power systems: Prony analysis, Matrix Pencil (MP), and Eigensystem Realization Algorithm (ERA) are examined.

The first part of this research discusses the optimal PMU placement (OPP) problem to find the optimal number of PMUs to make the system fully observable. Two different formulations are presented for modeling power grid observability to solve the OPP problem: mixed integer linear programming (MILP) and nonlinear programming (NLP). For each formulation, modeling of power flow measurements, zero injection, limited communication facility, single PMU failure, and limited channel capacity is studied. MILP zero injection formulation is improved to solve the redundant observability and optimality limitations. A new formulation for nonlinear programming-based PMU placement considering zero injection measurement is proposed. A comparison between MILP and NLP formulations is conducted to show the advantages and disadvantages of each formulation.

The second part of this research is to rank PMU measurements for oscillation monitoring based on two approaches: oscillation mode observability and Prony analysis. In the first approach, the system model is assumed known and the critical oscillation mode observability of different measurements are compared. In the second approach, the dynamic model of the system is not known. Prony analysis is employed to identify critical oscillation modes based on PMU measurements. Measurements at different locations are compared for their characteristics in Prony analysis. Specifically, singular values of Hankel matrices are compared. The two approaches lead to the same conclusion. Their internal connection is presented in this research. As a step further, sensitivity analysis of model order assumption and noise level in Prony analysis is conducted to show singular values of Hankel matrices can indeed serve as indicators of the quality of oscillation monitoring.

In addition, power system eigenvalues from PMU measurement data are identified using Prony analysis, matrix Pencil (MP), and Eigensystem Realization Algorithm (ERA). This part sheds insight on the principles of the three methods: eigenvalue identification through various Hankel matrix formulation. Further, multiple channel data handling and noise resilience techniques are investigated. In the literature, singular value decomposition (SVD)-based rank reduction technique has been applied to MP and resulted in a reduced-order system eigenvalue estimation and an excellent noise resilient feature. In this part of the research, ERA is refined using the SVD-based rank reduction to achieve a superior performance. Moreover, a reduced-order Prony analysis method is invented. With the proposed technique, Prony analysis can not only give reduced-order system eigenvalues, but also become noise resilient.

This dissertation has been resulted in three conference papers (two published and one accepted) and two journal papers (one published and one in revision process). The future work of this dissertation will examine the dynamic parameter estimation technique using the measurement-based methods. Using the PMU data and measurement-based methods of the

system identification can provide an accurate dynamic parameter estimation without prior information of the system transfer function. Generator parameters such as inertia constant, damping coefficients, and regulation speed constant can be estimated.

Chapter 1: Introduction

1.1 Background

Power system security needs to have a real-time monitor for situation awareness of the operating conditions of the system. In a control center, the state estimator deals with the measurements received from the remote terminal units (RTUs) at the substations and gives the best system state variables. Those measurements include bus voltages, branch currents, real and reactive power flows, and power injections. Recently, phasor measurement units (PMUs) with time tags from global positioning system (GPS) can provide synchronized phasor measurements of voltages and currents [1,2]. PMUs provide better situation awareness due to their much faster sampling rate (30 ~ 120 Hz) [3]. PMUs have been put into power grid for real-time monitoring. PMU installation at the power system has been rapidly increased in the recent years as shown in Fig. 1.1. According to the U.S. Department of Energy (2018), more than 2500 PMUs are installed in the U.S. power systems compared to 1700 in 2015. With this rapid increase, the analysis and identification of the PMU measurements for steady state and dynamic model estimation are of practical interest. The objective of this research is to investigate PMU issues including optimal PMU placement, PMU data for oscillation monitoring, and PMU measurements for eigenvalue estimation.

1.2 Phasor Measurement Unit (PMU)

Phasor measurement unit (PMU)-based sensors are used to collect time-stamped measurements from global positioning system (GPS) [1,2]. PMU sensors obtain synchronized

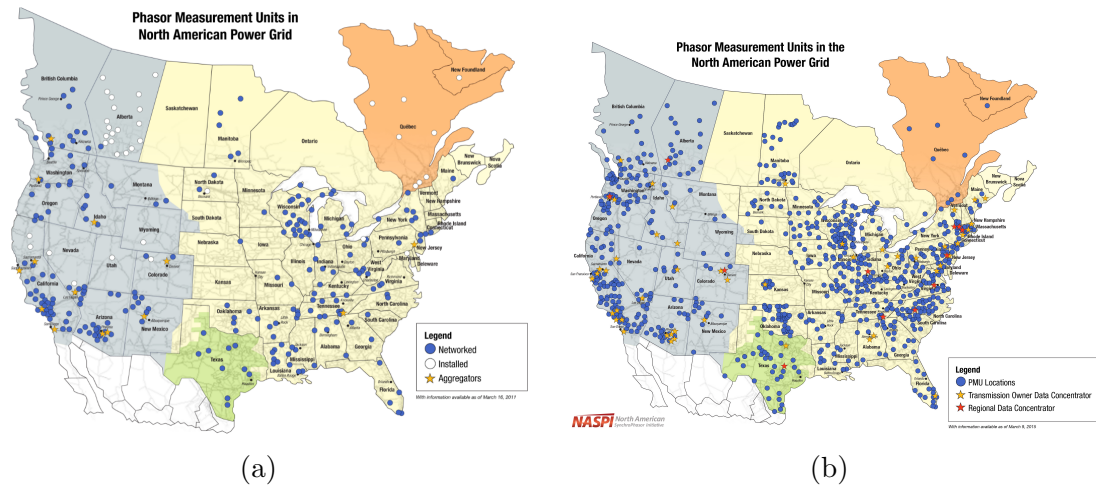


Figure 1.1: PMU locations in North American power grid. (a)2011. (b)2015. Maps courtesy of the North American SynchroPhasor Initiative and the U.S. Department of Energy [4]. Permission is included in Appendix B.

voltage and current phasors measurements at a faster rate of $30 \sim 120$ Hz and can give a superior situation awareness of the power grid [3]. PMU hardware block diagram consists of analog-to-digital converter, phase-locked oscillator, GPS receiver, anti-aliasing filters, and microprocessor as shown in Fig. 1.2 [5]. The analog AC waveforms are filtered out and digitized using anti-aliasing filter (above Nyquist rate) and analog-to-digital converter, respectively. The GPS pulse per second is converted into a high speed timing pulses sequence through the phase-locked oscillator. Discrete Fourier Transform phasor calculation is obtained by the microprocessor. Then data concentrator can provide the time-stamped phasor measurements.

1.3 Optimal PMU Placement (OPP)

Although PMUs are superior devices for improving the power system security, installing PMUs at every substation in the system is expensive and uneconomical. According to the U.S. Department of Energy, the overall cost of one PMU installation (including communication, security, labor, and equipment) is ranged from \$40,000 - \$180,000 as shown in Fig.

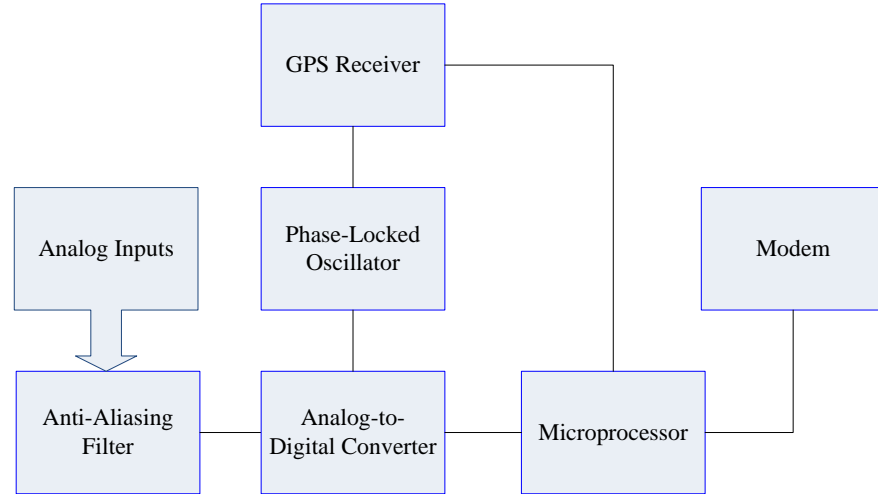


Figure 1.2: Phasor measurement unit block diagram.

1.3 [6]. When a PMU is placed at one bus, it can measure the voltage phasor of the bus and current phasors of all lines connected to that bus making the system observable [7]. Therefore, optimal PMU placement (OPP) problem should be solved to make the system entirely observable by installing less PMU devices at specific buses. In the literature, optimal PMU placement is solved using two techniques which are heuristic-based and mathematical programming-based. Mathematical programming-based methods are developed with two main formulations: MILP-based and nonlinear programming-based. This research proposes a new effective zero injection formulation in nonlinear programming to provide the minimum number of PMUs compared to other methods. Further, it improves MILP zero injection formulation to solve the observability redundancy and optimality drawbacks.

1.4 PMU for Inter-Area Oscillation Identification and Eigenvalue Estimation

Phasor measurement units have enhanced the accuracy of power grid real-time monitoring. Using PMU data for inter-area oscillation identification has been studied in the literature, and an IEEE PES taskforce report [8] has been published in 2012. Power system

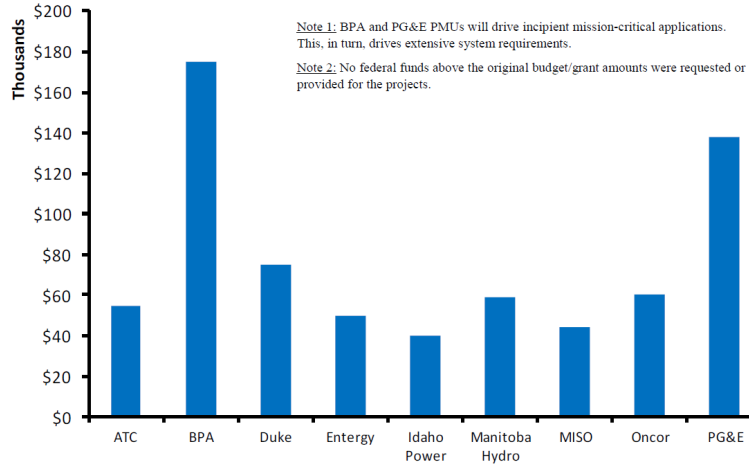


Figure 1.3: Phasor measurement unit installation cost. Reference: U.S. Department of Energy - Office of Electricity Delivery and Energy Reliability [6]. Permission is included in Appendix B.

models are nonlinear and complex systems. The modal information is identified from the system response to a perturbation to produce an adequate reduced order model. Prony analysis, matrix Pencil, and Eigensystem Realization Algorithm (ERA) are measurement-based identification methods for ringdown signals captured for a transient event [9]. This research contribution is categorized into two main parts. In the first part, the PMU measurements are ranked for oscillation monitoring based on two approaches which are oscillation mode observability and Prony analysis. The critical oscillation modes based on PMU measurements are identified using Prony analysis. The Hankel matrix singular values of the PMU measurements at different locations are compared. In the second part, ERA method is refined by applying SVD-based rank reduction on both Hankel matrices to achieve superior performance. A reduced-order Prony analysis method through Hankel matrix rank reduction is invented. The new Prony analysis can accurately identify system eigenvalues from noisy signals.

1.5 Outline of the Dissertation

This dissertation is organized as follows. Chapter 2 focuses on the optimal PMU placement problem using mixed integer linear programming and nonlinear programming. Power flow and zero injection measurement modeling along with restricted communication facilities, PMU failure, and limited channel capacity contingencies are investigated. MILP zero injection formulation to overcome the observability redundancy and optimality drawbacks and a new formulation for nonlinear programming-based PMU placement for zero injection measurement are proposed. Chapter 3 discusses the PMU measurements oscillation monitoring using Prony analysis and oscillation mode observability. PMU measurements ranking for oscillation monitoring is proposed. Chapter 4 investigates Prony analysis, Matrix Pencil (MP), and Eigensystem Realization Algorithm (ERA) for identifying power system eigenvalues from PMU measurement data. The multiple channel data and noise resilience techniques for the three methods are investigated. An improved ERA using SVD-based rank reduction and a reduced-order Prony analysis to provide superior results are proposed. Chapter 5 concludes the dissertation and presents the future work.

Chapter 2: Optimal PMU Placement for Steady State Estimation

2.1 Introduction

The power system is required to have a real-time monitoring of the system operating conditions to enhance its security. In power grids, the measured bus voltage, currents, real and reactive power are collected by remote terminal units at each substation. Those measurements are sent to a control center. A control center then conducts state estimation to determine the best estimates of system's state variables (every node's voltage magnitude and phase angle). Most recently, phasor measurement unit (PMU)-based sensors are used to collect time-stamped measurements from global positioning system (GPS) [1, 2]. PMU sensors obtain synchronized voltage and current phasors measurements at a faster rate of (30 ~ 120 Hz) [3]. Hence, PMUs can give a superior situation awareness of the power grid. By installing a PMU at one bus, it can obtain the bus voltage phasor and all current phasors of the branches connected to that bus [7]. However, placing PMU sensors at all buses of the system can be expensive and uneconomical. Therefore, optimal PMU placement (OPP) problem is investigated in this chapter ¹ to make the system entirely observable by installing less PMU devices at specific buses.

Heuristic and mathematical programming techniques are used to solve the OPP problem. The heuristic technique is based on search process to obtain the OPP. There are several heuristic-based techniques that have been studied in the literature. A graph theory and simulated annealing algorithm to obtain the minimum number of PMU sensors are developed

¹This chapter was published in International Transactions on Electrical Energy Systems [10], 2019. Permission is included in Appendix B.

in [11]. Then other heuristic-based approaches have been proposed such as simulated annealing with Tabu search [12], spanning tree [13], genetic algorithm [14], nondominated sorting genetic [15], Tabu search genetic [16], particle swarm optimization approach [17], and recursive Tabu search [18]. An immunity genetic algorithm [19] and binary particle swarm optimization [20,21] are used to solve the OPP problem.

Heuristic-based OPP does not guarantee a global optimum solution. Hence, two major mathematical programming approaches are developed in the literature: MILP and NLP. While MILP formulations guarantee a global optimum solution, NLP formulations provide several local minimum solutions.

Integer linear programming (ILP) to obtain the OPP is introduced in [2,7]. Several algorithms and techniques considering integer linear programming and contingency-constrained PMU placement are developed in [22–28]. In [29], ILP is used with auxiliary variable to find the OPP in case of zero injection. The same method considering conventional measurements is developed in [30]. Zero injection redundancy limitation and global optimal solution considering mutual buses are presented in [31]. Reference [32] proposes an integer quadratic programming approach. A weighted least square algorithm using nonlinear observability constraint is presented in [33]. Nonlinear programming (NLP) formulations are introduced in [34]. This type of formulations has been explored under several contingencies in [35,36]. In [37], MILP and NLP comparison is conducted using a simple system, and limitation of zero injection formulation for NLP is discussed. However, zero injection formulation in nonlinear programming-based PMU placement has not been properly solved in the literature.

In this chapter, modeling power grid observability to solve the OPP problem is implemented using two different approaches which are MILP and NLP. Power flows, zero injections, restricted communication facilities, PMU failure, and limited channel capacity are discussed. A new nonlinear programming formulation for zero injection is proposed. The proposed formulation is examined by validating the results with the MILP formulation. MILP and

NLP comparison is conducted to illustrate their advantages and disadvantages. The main contributions of this chapter can be summarized as follows. First, a new effective zero injection formulation in nonlinear programming is proposed and validated to provide minimum number of PMUs compared to other methods. Second, MILP zero injection formulation is improved to solve the observability redundancy and optimality drawbacks. Third, two mathematical programming methods are compared under several contingencies applied to different IEEE test systems, and the proposed zero injection formulations are evaluated on a large 2383-bus Polish system.

The rest of this chapter is organized as follows. Sections 2.2 and 2.3 present MILP and NLP formulations. Section 2.4 proposes the effective power flow and zero injection measurement formulations and investigates the aforementioned contingencies. Section 2.5 concludes this chapter.

2.2 Mixed Integer Linear Programming

Power system state estimation with a DC power flow is analyzed in this chapter, and (2.1) presents the linear measurement function which maps the state to the measurement.

$$z = Hx + e \quad (2.1)$$

where z represents the measurement vector, H is the measurement matrix, x is the state variable vector, and e is the error measurement vector. The state variables are the voltage phase angle for each bus in the power system. The PMUs can obtain the measurements including the voltage phase angle (θ_i) of Bus i and the power flow from Bus i to Bus j , where $j \in ad_i$ represents the adjacent buses to Bus i . Thus, the PMU will measure θ_i , and θ_j can be obtained as the power flow P_{ij} is measurable. Therefore, Bus i with its adjacent buses are observable when a PMU is installed only at Bus i .

In other words, Bus i itself can be observable with at least a single PMU placed at this bus or one of its adjacent buses. This is can be represented by the following inequality:

$$f_i(x) = x_i + \sum_{j \in ad_i} x_j \geq 1 \quad (2.2)$$

where $f_i(x)$ is the observability function for Bus i , x_i is a binary decision variable to install a PMU at Bus i ($x_i = 1$) or not ($x_i = 0$), and x_j is the binary decision variable for the buses adjacent to that bus.

The OPP for the IEEE 14-bus system (shown in Fig. 2.1) [38] is formulated as the following:

$$\begin{aligned} \min_x \quad & \sum_{k=1}^{14} x_k \\ \text{subject to:} \quad & f_i(x) \geq 1 \\ & x_i \in \{0, 1\}, i = 1, 2, \dots, 14. \end{aligned}$$

where

$$f_i(x) = \begin{cases} f_1 = x_1 + x_2 + x_5 \geq 1, & f_2 = x_1 + x_2 + x_3 + x_4 + x_5 \geq 1, \\ f_3 = x_2 + x_3 + x_4 \geq 1, & f_4 = x_2 + x_3 + x_4 + x_5 + x_7 + x_9 \geq 1, \\ f_5 = x_1 + x_2 + x_4 + x_5 + x_6 \geq 1, & f_6 = x_5 + x_6 + x_{11} + x_{12} + x_{13} \geq 1, \\ f_7 = x_4 + x_7 + x_8 + x_9 \geq 1, & f_8 = x_7 + x_8 \geq 1, \\ f_9 = x_4 + x_7 + x_9 + x_{10} + x_{14} \geq 1, & f_{10} = x_9 + x_{10} + x_{11} \geq 1, \\ f_{11} = x_6 + x_{10} + x_{11} \geq 1, & f_{12} = x_6 + x_{12} + x_{13} \geq 1, \\ f_{13} = x_6 + x_{12} + x_{13} + x_{14} \geq 1, & f_{14} = x_9 + x_{13} + x_{14} \geq 1 \end{cases}$$

This OPP problem is formulated as MILP and solved by MATLAB's *intlinprog* function. The OPP result indicates that only four PMUs can be installed on buses 2, 8, 10, and 13 to make the system entirely observable. Generalized MILP can be expressed as [7]:

$$\min_x \sum_{k=1}^N w_k x_k \quad (2.3a)$$

$$\text{subject to: } Ax \geq B \quad (2.3b)$$

$$x_i \in \{0, 1\}, i = 1, \dots, N \quad (2.3c)$$

where x_i is the binary decision, and w_k is the PMU placement cost. It is assumed that the PMUs have the placement cost $w_i = 1$ making the PMU placement cost minimization equivalent to the number of PMUs minimization. Entries of A and the B matrices are:

$$a(i, j) = \begin{cases} 1, & \text{Bus } i \text{ and Bus } j \text{ are connected} \\ 1, & i \text{ is equal to } j \\ 0. & \text{Otherwise} \end{cases}$$

$$B = \begin{bmatrix} 1 & 1 & \dots & 1 \end{bmatrix}^T$$

2.3 Nonlinear Programming

OPP problem can be formulated and solved using nonlinear programming (NLP) which based on sequential quadratic programming (SQP) [33,34]. NLP method can produce more than one solution to the OPP problem, while the MILP formulation can provide a single solution.

For NLP, x_i is considered as a continuous decision variable rather a binary variable as the MILP formulation. Therefore, x_i is forced to be 1 or 0 by the following constraint: $x_i(x_i - 1) = 0$.

The quadratic objective function, which represents the overall PMU placement cost, is minimized by the NLP formulation subjected to nonlinear equality constraints. The decision variables are 0 and 1 which indicate the lower and upper bounds of the problem formulation. Hence, the nonlinear constraints can assure the complete observability of the system [33,34].

The NLP formulation for the OPP problem can be expressed as:

$$\min_x J(x) = x^T W x = \sum_{k=1}^N w_k x_k^2 \quad (2.4a)$$

$$\text{s.t.: } g_i(x) = (1 - x_i) \prod_{j \in ad_i} (1 - x_j) = 0 \quad (2.4b)$$

$$0 \leq x_i \leq 1, \quad \text{for all } i \in \mathbf{S} \quad (2.4c)$$

where $J(x)$ represents the OPP objective function, x^T is the transposed vector of x , W is the diagonal weight matrix, ad_i indicates the adjacent buses of Bus i , and \mathbf{S} represents the system buses set.

This NLP formulation is a nonconvex optimization problem since a number of local minimum solutions can result in using the nonlinear equality constraints [34], and it is solved by sequential quadratic programming (SQP) algorithm. As a consequence, several solutions for the OPP problem can be obtained by choosing different initial conditions x .

The IEEE 14-bus system [38] as shown in Fig. 2.1 is used as an example to solve the OPP problem with the NLP formulation, and the NLP and MILP solutions are compared to each other. The NLP is formulated as follows.

$$\begin{aligned}
& \min_x \sum_{k=1}^{14} x_k^2 \\
& \text{s.t.: } g_i(x) = (1 - x_i) \prod_{j \in ad_i} (1 - x_j) = 0 \\
& 0 \leq x_i \leq 1, \quad i = 1, 2, \dots, 14.
\end{aligned}$$

where $g_i(x)$ will be as follows.

$$g_i(x) = \begin{cases}
g_1 = (1 - x_1)(1 - x_2)(1 - x_5) = 0, \\
g_2 = (1 - x_2)(1 - x_1)(1 - x_3)(1 - x_4)(1 - x_5) = 0, \\
g_3 = (1 - x_3)(1 - x_2)(1 - x_4) = 0, \\
g_4 = (1 - x_4)(1 - x_2)(1 - x_3)(1 - x_5)(1 - x_7)(1 - x_9) = 0, \\
g_5 = (1 - x_5)(1 - x_1)(1 - x_2)(1 - x_4)(1 - x_6) = 0, \\
g_6 = (1 - x_6)(1 - x_5)(1 - x_{11})(1 - x_{12})(1 - x_{13}) = 0, \\
g_7 = (1 - x_7)(1 - x_4)(1 - x_8)(1 - x_9) = 0, \\
g_8 = (1 - x_8)(1 - x_7) = 0, \quad g_9 = (1 - x_9)(1 - x_4)(1 - x_7)(1 - x_{10})(1 - x_{14}) = 0, \\
g_{10} = (1 - x_{10})(1 - x_9)(1 - x_{11}) = 0, \quad g_{11} = (1 - x_{11})(1 - x_6)(1 - x_{10}) = 0, \\
g_{12} = (1 - x_{12})(1 - x_6)(1 - x_{13}) = 0, \\
g_{13} = (1 - x_{13})(1 - x_6)(1 - x_{12})(1 - x_{14}) = 0, \\
g_{14} = (1 - x_{14})(1 - x_9)(1 - x_{13}) = 0
\end{cases}$$

It is assumed that the weight of all PMUs is $w_i = 1$ to make the installation cost minimization equivalent to the number of PMUs minimization. The MATLAB's function *fmincon* is used to solve this nonconvex optimization problem with NLP formulation and SQP solver.

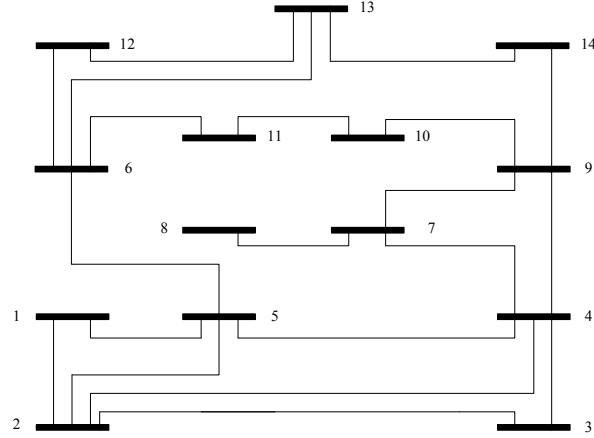


Figure 2.1: IEEE 14-bus system.

The NLP obtains various solutions to the OPP problem based on the initial points x . Therefore, the initial points are programmed to be random numbers in the feasible region between the upper and lower bounds of one and zero. As a result, optimal solutions are found after several iterations:

$$x = [0 \ 1 \ 0 \ 0 \ 0 \ 0 \ 0 \ 1 \ 0 \ 1 \ 0 \ 0 \ 1 \ 0]^T, \quad x = [0 \ 1 \ 0 \ 0 \ 0 \ 0 \ 1 \ 0 \ 0 \ 1 \ 0 \ 0 \ 1 \ 0]^T, \quad x = [0 \ 1 \ 0 \ 0 \ 0 \ 0 \ 1 \ 0 \ 0 \ 0 \ 1 \ 0 \ 1 \ 0]^T, \\ x = [0 \ 1 \ 0 \ 0 \ 0 \ 1 \ 0 \ 1 \ 1 \ 0 \ 0 \ 0 \ 0 \ 0]^T \text{ and } x = [0 \ 1 \ 0 \ 0 \ 0 \ 1 \ 1 \ 0 \ 1 \ 0 \ 0 \ 0 \ 0 \ 0]^T.$$

The above solutions indicate that the OPP buses are the following five sets: $\{2, 8, 10, 13\}$, $\{2, 7, 10, 13\}$, $\{2, 7, 11, 13\}$, $\{2, 6, 8, 9\}$, or $\{2, 6, 7, 9\}$. Note that the first optimal solution is the same as the MILP solution.

Thus, NLP is another effective algorithm to solve the OPP problem by obtaining various optimal solutions to select from. MILP and NLP comparison for the OPP problem is conducted using four different systems which are IEEE 14-, 57-, 118-, and 300-bus systems [38] as shown in Table 2.1.

Table 2.1: OPP results using MILP and NLP/SQP

IEEE Test System	Number of PMUs		Number of NLP Solutions
	MILP	NLP	
14-bus	4	4	5
57-bus	17	17	19
118-bus	32	32	10
300-bus	87	87	8

2.4 OPP Case Studies

2.4.1 Power Flow Measurements

Suppose that Branch ij in the system has a meter to measure the power flow. In the case that one of the state variables of Bus i or j (θ_i or θ_j) is measured, the state variable of the other bus can be provided since the power flow (P_{ij}) is known.

2.4.1.1 MILP Approach

With the information of the power flows, the observability constraints must be reformulated to find the optimal solution. If the power flow measurement on the Branch $i-j$ is not given, Bus i and Bus j have the following observability constraints:

$$f_i = \sum_k A_{ik} x_k \geq 1 \quad (2.5a)$$

$$f_j = \sum_k A_{jk} x_k \geq 1 \quad (2.5b)$$

When the power flow measurement on Branch k of Bus i and Bus j is known, the constraints (2.5a) and (2.5b) are modified to be a joint observability constraint as follows [7,24].

$$f_{flow,k} = f_i + f_j \geq 1 \quad (2.6)$$

Constraint (2.6) indicates that if Bus i or Bus j is observable, the other bus can also be observable since the power flow of Branch k is given.

2.4.1.2 NLP Approach

Similarly, the observability constraints of the nonlinear programming must be reformulated to find the optimal solution with the measured power flow. Therefore, the observability constraints of Bus i and Bus j are modified to be a joint observability constraint as the following [35]:

$$g_{flow,k} = g_i g_j = 0 \quad (2.7)$$

Constraint (2.7) can result in high orders since several terms of $(1 - x_i)$ can be produced with multiplying the constraints of Bus i and Bus j [35]. Hence, the resulted terms with high orders will be treated as a first order term since this constraint has a zero right hand side.

2.4.1.3 Power Flow Measurement Example

Suppose that the power flow measurements for the IEEE 14-bus system (Fig. 2.1) [38] are on branches 2 – 3, 3 – 4, 6 – 11, 6 – 12, and 7 – 8. Then constraints (2.6) and (2.7) are formulated for MILP and NLP for lines with flow measurements. The observability functions of buses 2, 3, and 4 for the MILP are:

$$f_2 = x_1 + x_2 + x_3 + x_4 + x_5 \geq 1, \quad f_3 = x_2 + x_3 + x_4 \geq 1,$$

$$f_4 = x_2 + x_3 + x_4 + x_5 + x_7 + x_9 \geq 1$$

The joint constraint (2.6) is applied since there are power flows on branches 2 – 3 and 3 – 4:

$$\begin{aligned} f_{flow,2-3,3-4} &= f_2 + f_3 + f_4 \geq 1 \\ &= x_1 + 3x_2 + 3x_3 + 3x_4 + 2x_5 + x_7 + x_9 \geq 1 \end{aligned}$$

Joint constraint $f_{flow,2-3,3-4}$ means that only one of the buses 2, 3, and 4 must be observable to make the other buses observable since the power flows are known. Hence, this joint constraint meets the minimum requirement of installing at least a single PMU at one of those buses or at the buses adjacent to them.

Likewise, the observability functions of buses 6, 11, and 12 are:

$$f_6 = x_5 + x_6 + x_{11} + x_{12} + x_{13} \geq 1, \quad f_{11} = x_6 + x_{10} + x_{11} \geq 1, \quad f_{12} = x_6 + x_{12} + x_{13} \geq 1$$

Then the above three constraints are merged into a joint constraint as follows.

$$f_{flow,6-11,6-12} = x_5 + 3x_6 + x_{10} + 2x_{11} + 2x_{12} + 2x_{13} \geq 1$$

The third joint constraint for Branch 7 – 8 is obtained in a similar way as follows.

$$f_{flow,7-8} = x_4 + 2x_7 + 2x_8 + x_9 \geq 1$$

For the nonlinear programming, the observability functions for buses 2, 3, and 4 are:

$$g_2 = (1 - x_2)(1 - x_1)(1 - x_3)(1 - x_4)(1 - x_5) = 0,$$

$$g_3 = (1 - x_3)(1 - x_2)(1 - x_4) = 0,$$

$$g_4 = (1 - x_4)(1 - x_2)(1 - x_3)(1 - x_5)(1 - x_7)(1 - x_9) = 0$$

Joint constraint (2.7) is applied to the three observability functions due to the power flows on branches 2 – 3 and 3 – 4:

$$g_{flow,2-3,3-4} = g_2 g_3 g_4 = 0$$

$$= (1 - x_1)(1 - x_2)(1 - x_3)(1 - x_4)(1 - x_5)(1 - x_7)(1 - x_9) = 0$$

In a similar way, power flow joint constraints for branches 6 – 11, 6 – 12, and 7 – 8 are obtained as the following:

$$g_{flow,6-11,6-12} = g_6 g_{11} g_{12} = (1 - x_5)(1 - x_6)(1 - x_{10})(1 - x_{11})(1 - x_{12})(1 - x_{13}) = 0$$

$$g_{flow,7-8} = g_7 g_8 = (1 - x_4)(1 - x_7)(1 - x_8)(1 - x_9) = 0$$

Table 2.2 shows the results of the OPP for power flow case. The number of PMUs in this case is reduced due to the power flow meters. Table 2.3 presents the location of the power flow measurement branches.

Table 2.2: Power flow measurements case results

IEEE Test System	Number of Flow Branches	Number of PMUs		Number of NLP Solutions
		MILP	NLP	
14-bus	5	3	3	11
57-bus	40	6	6	5
118-bus	31	24	24	5
300-bus	43	81	81	4

2.4.2 Zero Injection Measurements

A four-bus system as illustrated in Fig. 2.2 is used to easily demonstrate the zero injection case. To have each of the four buses observable, the following constraints should be satisfied in the MILP and NLP formulations, respectively.

Table 2.3: Branches of power flow measurements

IEEE Test System	Branches of Flow Measurements
14-bus	2-3,3-4,6-11,7-8,6-12
57-bus	1-2,1-15,1-16,1-17,3-15,4-5,4-6,4-18,7-29, 29-52,8-9,9-10,10-12,10-51,12-13,51-50, 11-41,11-43,41-42,42-56,14-46,47-46, 19-20,20-21,22-38,38-37,38-44,38-48, 49-38,23-24,24-25,24-26,27-26,28-27, 30-31,32-34,34-35,36-35,40-36,53-54
118-bus	1-3,3-5,6-7,8-9,11-13,16-17,20-21,23-25, 23-32,32-114,27-28,34-43,35-36,41-42, 47-46,49-50,50-57,51-52,56-58,60-62, 65-68,68-116,71-73,76-77,77-82,82-83, 86-87,90-91,95-96,99-100,110-112
300-bus	1-3,3-4,6-7,8-11,11-13,15-16,21-22,24-25, 25-26,32-35,37-38,40-68,68-174,46-47, 50-51,55-56,70-71,77-84,84-86,95-103, 108-112,120-125,136-138,145-265, 156-157,160-166,166-167,173-198, 198-216,216-220,182-190,184-185, 200-202,208-209,88-235,64-239,2-248, 17-252,109-263,270-292,270-296, 269-288,294-300

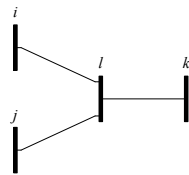


Figure 2.2: Four-bus system.

$$\text{MILP: } f_i \geq 1, f_j \geq 1, f_k \geq 1, f_l \geq 1 \quad (2.8)$$

$$\text{NLP: } g_i = 0, g_j = 0, g_k = 0, g_l = 0 \quad (2.9)$$

Now assume that Bus ℓ has a zero injection measurement. The power injection and the voltage phase angles of the four buses are related to each other as the following:

$$P_{inj,l} = \frac{\theta_l - \theta_i}{X_{li}} + \frac{\theta_l - \theta_j}{X_{lj}} + \frac{\theta_l - \theta_k}{X_{lk}} = 0 \quad (2.10)$$

If the power injection and three of the phase angles are known, the fourth phase angle can be measured. Therefore, three buses have to be observable to make the fourth one observable with the help of the installed PMU and the zero injection at Bus ℓ . This requirement is formulated using the MILP as [7]:

$$f_{inj,l} = f_i + f_j + f_k + f_l \geq 3 \quad (2.11)$$

When one of the observability functions (f_i, f_j, f_k , or f_l) equals to zero, then the joint constraint (2.11) meets the zero injection requirement. Nevertheless, this joint constraint may result in two drawbacks. First, adding the observability functions can produce a redundancy for certain buses which can make the constraint (2.11) satisfied with two zero

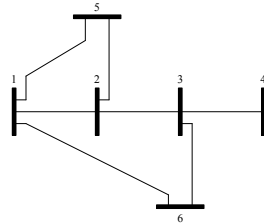


Figure 2.3: Six-bus system.

observability functions [31]. A six-bus system (shown in Fig. 2.3) is employed to explain the drawbacks of the constraint (2.11). Assume that Bus 2 has a zero injection measurement. Three buses (1, 3, and 5) are adjacent to Bus 2. Thus, the MILP constraints for this system will be as follows.

$$\begin{aligned} f_{inj,2} &= f_1 + f_2 + f_3 + f_5 \geq 3 \\ &= 3x_1 + 4x_2 + 2x_3 + x_4 + 3x_5 + 2x_6 \geq 3 \\ f_4 &= x_3 + x_4 \geq 1, \quad f_6 = x_1 + x_3 + x_6 \geq 1 \end{aligned}$$

From the above constraints, the OPP can be on buses 3 and 4 (i.e. $f_1 = 0$, $f_2 = 1$, $f_3 = 2$, $f_4 = 2$, $f_5 = 0$, and $f_6 = 1$) which leaves buses 1 and 5 unobservable. Note that the two buses 1 and 5 cannot be observable even with the help of zero injection measurement since two out of four buses are unobservable. Therefore, the system complete observability is not guaranteed in some configuration.

Recently, it has been clarified in [31] that f_i cannot be guaranteed to be 0 or 1 which is the main reason of this limitation. For example, f_j and f_k can be 2, while f_i and f_l can be 0 which satisfy (2.11). For that reason, the constraint (2.11) does not guarantee at least 3 out of 4 buses are observable. Thus, the authors propose a formulation to keep the right hand side equals to 1 which can solve the redundant observability of some buses. Then the joint constraint (2.11) is reformulated as follows.

$$f_{inj,l} = \left\{ \begin{array}{l} f_i + f_j \geq 1, \quad f_i + f_k \geq 1, \quad f_i + f_l \geq 1, \quad f_j + f_k \geq 1, \quad f_j + f_l \geq 1, \quad f_k + f_l \geq 1 \end{array} \right. \quad (2.12)$$

The observability constraint (2.12) guarantees complete observability since it can be satisfied if at most one of the observability constraints (f_i, f_j, f_k , or f_l) is zero.

Solving the same problem using (2.12), then the MILP constraints will be as the following:

$$f_{inj,2} = \left\{ \begin{array}{l} f_1 + f_2 \geq 1, \quad f_1 + f_3 \geq 1, \quad f_1 + f_5 \geq 1, \quad f_2 + f_3 \geq 1, \quad f_2 + f_5 \geq 1, \quad f_3 + f_5 \geq 1 \end{array} \right.$$

$$f_4 = x_3 + x_4 \geq 1$$

$$f_6 = x_1 + x_3 + x_6 \geq 1$$

From the above constraints, the optimal PMU placement can be on buses 3 and 6 (i.e. $f_1 = 1, f_2 = 1, f_3 = 2, f_4 = 1, f_5 = 0,$ and $f_6 = 2$) which leaves Bus 5 unseen by the PMUs but can be observable with the help of zero injection measurement at Bus 2.

In addition to the redundant observability, the joint constraint (2.11) cannot obtain the optimum solution if there are two or more zero injections with mutual buses [31]. Assume that there are zero injections at Bus 1 and Bus 3 in the six-bus system (shown in Fig. 2.3). The adjacent buses to Bus 1 are buses 2, 5, and 6, while the adjacent buses to Bus 3 are buses 2, 4, and 6. In this case, Bus 2 and Bus 6 are mutual buses, then MILP constraints using (2.11) can be as the following:

$$\begin{aligned} f_{inj,1} &= f_1 + f_2 + f_5 + f_6 \geq 3 \\ &= 4x_1 + 3x_2 + 2x_3 + 3x_5 + 2x_6 \geq 3 \end{aligned}$$

$$\begin{aligned} f_{inj,3} &= f_2 + f_3 + f_4 + f_6 \geq 3 \\ &= 2x_1 + 2x_2 + 4x_3 + 2x_4 + x_5 + 2x_6 \geq 3 \end{aligned}$$

These constraints can be satisfied using at least two PMUs (e.g., placement at Bus 1 and Bus 3), while this problem can be satisfied using only one PMU at Bus 2. Note that by placing a single PMU at Bus 2, Bus 4 and Bus 6 are unseen by the PMU but can be observable with the zero injections at Bus 1 and Bus 3. Therefore, the optimal solution

may not be provided using the joint constraint (2.11). This problem can be solved using (2.12) with some modification [31]. Suppose that Bus 1 and Bus 3 have zero injections in the six-bus system (Fig. 2.3). The MILP constraints using (2.12) will be as follows.

$$f_{inj,1} = \left\{ f_1 + f_2 \geq 1, f_1 + f_5 \geq 1, f_1 + f_6 \geq 1, f_2 + f_5 \geq 1, f_2 + f_6 \geq 1, f_5 + f_6 \geq 1 \right.$$

$$f_{inj,3} = \left\{ f_2 + f_3 \geq 1, f_2 + f_4 \geq 1, f_2 + f_6 \geq 1, f_3 + f_4 \geq 1, f_3 + f_6 \geq 1, f_4 + f_6 \geq 1 \right.$$

Then mutual observability functions in the left-hand side of $f_{inj,1}$ and $f_{inj,3}$ have to be merged. In this chapter, the MILP formulation is improved by solving the optimality limitation with less constraints as the following:

$$f_{inj,1 \text{ and } 3} = \left\{ \begin{array}{l} f_1 + f_2 + f_3 \geq 1, f_1 + f_2 + f_4 \geq 1, f_1 + f_3 + f_6 \geq 1, f_1 + f_4 + f_6 \geq 1, \\ f_2 + f_3 + f_5 \geq 1, f_2 + f_4 + f_5 \geq 1, f_3 + f_5 + f_6 \geq 1, f_4 + f_5 + f_6 \geq 1, \\ f_1 + f_5 \geq 1, f_3 + f_4 \geq 1, f_2 + f_6 \geq 1 \end{array} \right.$$

These constraints can obtain the OPP by placing a single PMU at Bus 2 after merging the mutual observability functions. With zero injections at Bus 1 and Bus 3, observability can be assured for Bus 4 and Bus 6. The number of constraints in [31] to solve the six-bus system is 16 compared to 11 in this chapter. This reduction in the number of the constraints is significant for solving large systems.

For the NLP formulation, the equivalent has not been addressed adequately. The zero injection joint constraint for NLP in [35] is not equivalent to (2.11) or (2.12). It indicates that the zero injection bus and its adjacent buses are observable if one of them is observable. As a consequence, this constraint can result in unobservable buses. In this section, the equivalent in nonlinear programming formulation is proposed.

Once Bus ℓ has a zero injection measurement (Fig. 2.2), for this particular case, then we need at least any 3 buses among all 4 buses to be observable to guarantee a complete observability.

That is, the following six constraints should be satisfied.

$$g_{inj,l} = \left\{ g_i g_j = 0, \quad g_i g_k = 0, \quad g_i g_l = 0, \quad g_j g_k = 0, \quad g_j g_l = 0, \quad g_k g_l = 0 \right. \quad (2.13)$$

Suppose that Bus 2 has a zero injection in the six-bus system (shown in Fig. 2.3). Buses 1, 3, and 5 are adjacent buses to Bus 2. The NLP constraints will be as follows.

$$g_{inj,2} = \left\{ g_1 g_2 = 0, \quad g_1 g_3 = 0, \quad g_1 g_5 = 0, \quad g_2 g_3 = 0, \quad g_2 g_5 = 0, \quad g_3 g_5 = 0 \right.$$

$$g_4 = (1 - x_3)(1 - x_4) = 0$$

$$g_6 = (1 - x_1)(1 - x_3)(1 - x_6) = 0$$

Then an optimal solution can be achieved by installing PMUs on Bus 3 and Bus 6 (i.e. $g_1 = 0, g_2 = 0, g_3 = 0, g_4 = 0, g_5 = 1, \text{ and } g_6 = 0$) which makes Bus 5 cannot be seen by the PMUs but can be observable with the help of Bus 2 zero injection measurement.

Then suppose that Bus 1 and Bus 3 have zero injections in the same aforementioned system. The NLP constraints with the mutual buses will be as follows.

$$g_{inj,1 \text{ and } 3} = \left\{ \begin{array}{l} g_1 g_2 g_3 = 0, \quad g_1 g_2 g_4 = 0, \quad g_1 g_3 g_6 = 0, \quad g_1 g_4 g_6 = 0, \\ g_2 g_3 g_5 = 0, \quad g_2 g_4 g_5 = 0, \quad g_3 g_5 g_6 = 0, \quad g_4 g_5 g_6 = 0, \\ g_1 g_5 = 0, \quad g_3 g_4 = 0, \quad g_2 g_6 = 0 \end{array} \right.$$

From these constraints, the optimal PMU placement can be at Bus 2. Note that buses 4 and 6 are observable with the zero injection measurements at buses 1 and 3.

Thus, both MILP and NLP joint constraints for zero injection measurements can be satisfied if at most one of the observability constraints (zero injection bus or its adjacent buses constraints) is zero. Also, these joint constraints guarantee complete observability and optimal solution to the problem. Table 2.4 and Table 2.5 show the location of the zero injections and the results of the zero injection case for MILP and NLP, respectively.

Table 2.4: Zero injection measurement locations

IEEE Test System	Zero Injection Measurement Buses
14-bus	7
57-bus	4,7,11,21,22,24,26,34,36,37,39,40,45,46,48
118-bus	5,9,30,37,38,63,64,68,71,81
300-bus	17,58,233,256,294

Table 2.5: Zero injection case results

IEEE Test System	Number of Zero Injections	Number of PMUs		Number of NLP Solutions
		MILP	NLP	
14-bus	1	3	3	1
57-bus	15	11	11	6
118-bus	10	28	28	4
300-bus	5	82	82	2

2.4.3 Limited Communication Facility

PMUs need to communicate with the control center through data links at the substations to provide the measurements of synchronized voltage and current phasors. Therefore, a substation with limited communication facility can obstruct the PMU placement. With restricted communication problem, the PMU placement cost will be increased [39]. Hence, the placement cost w_i for MILP and NLP will be increased for any bus with limited communications. As a result, this high placement cost can omit the limited communication buses

from the optimal solution [35]. Suppose that Bus 2 and Bus 9 have limited communication facilities on the IEEE 14-bus system (shown in Fig. 2.1) [38]. Then the placement costs of Bus 2 and Bus 9 are increased to be $w_i = 10^9$. Table 2.6 shows the results of the limited communication facility case.

Table 2.6: Limited communication facility case results

IEEE Test System	Limited Communication Buses	Number of PMUs		Number of NLP Solutions
		MILP	NLP	
14-bus	2,9	5	5	11
57-bus	1,4,9,15	17	17	10
118-bus	2,9,11,12,17	35	35	8
300-bus	2,9,11,64,111, 277,299,300	92	92	4

2.4.4 Single PMU Failure

Even though the PMUs have a high reliability, there is a chance of a single PMU failure. To assure the complete observability of the system, main and backup sets are obtained. The optimal PMU solution without taking the PMU failure into account is the main set, whereas the backup set is generated in case of a PMU failure. The right hand side of the MILP constraints can be modified to be two to let each bus observed by two PMUs [22]. Instead, the main set terms x_i and x_j of the MILP constraints can be removed to generate the backup set. Likewise, the main set terms $(1 - x_i)$ and $(1 - x_j)$ of the NLP constraints are removed to provide the backup set [35]. Therefore, the buses in the main set will not be selected again, and the backup set will assure the complete observability of the system when a one PMU fails.

IEEE 14-bus system (Fig. 2.1) main set is obtained as in Section 2.2 and Section 2.3, and then MILP and NLP main set can be the following: $\{2, 8, 10, 13\}$. Therefore, all of the terms x_2 , x_8 , x_{10} , and x_{13} of MILP constraints are ignored to generate the backup set. Similarly,

all of the terms $(1 - x_2)$, $(1 - x_8)$, $(1 - x_{10})$, and $(1 - x_{13})$ are removed from the NLP constraints.

After solving the problem, the resulted backup set for the MILP is $\{1, 4, 6, 7, 9\}$, whereas the backup sets for the NLP formulation are $\{1, 4, 6, 7, 9\}$, $\{1, 3, 6, 7, 9\}$, $\{3, 5, 6, 7, 9\}$, or $\{4, 5, 6, 7, 9\}$. From Table 2.7, we can see that the single PMU failure case would double the total minimum number of PMUs due to the backup set.

Table 2.7: Single PMU failure results

IEEE Test System	Number of PMUs		Number of NLP Solutions
	MILP	NLP	
14-bus	9	9	4
57-bus	35	35	4
118-bus	75	75	2
300-bus	221	221	2

2.4.5 Limited PMU Channel Capacity

The OPP has been solved supposing that all PMUs have enough channels to make all adjacent buses observable. In reality, PMUs are made to have a different number of channels with different prices [25]. In this section, the OPP is analyzed in case that we have PMUs with limited channel capacity.

Let's assume that the number of adjacent buses to Bus i (m_i) is larger than the PMU channel capacity (c). The number of line combinations ($C_{m_i}^c$) is given as follows [35, 36].

$$C_{m_i}^c = \frac{m_i!}{c!(m_i - c)!} \quad (2.14)$$

Then the observability constraints are changed for both MILP and NLP to meet the possible line combinations. Note that if the number of adjacent buses to Bus i is less than

or equal to the number of channel capacity, the observability constraint of Bus i is kept the same.

Let's assume that we have PMUs with limited channel capacity where $c = 3$ for the 14-bus system (Fig. 2.1). Then the observability constraints are changed as follows.

- At Bus 1:

The adjacent buses are 2 and 5 which means that $m_1 = 2$ and $c > m_1$. Thus, we have enough channels for this bus, and the constraints f_1 and g_1 are kept the same.

- At Bus 2:

The adjacent buses are 1, 3, 4, and 5 which means that $m_2 = 4$ and $c < m_2$. Thus, the number of line combinations is 4, and they are $\{2 - 1, 2 - 3, 2 - 4\}$, $\{2 - 1, 2 - 3, 2 - 5\}$, $\{2 - 1, 2 - 4, 2 - 5\}$, and $\{2 - 3, 2 - 4, 2 - 5\}$. Then the observability constraint for Bus 2 is changed as follows.

- For MILP:

$$f_{2,1} = x_2 + x_1 + x_3 + x_4 \geq 1, \quad f_{2,2} = x_2 + x_1 + x_3 + x_5 \geq 1$$

$$f_{2,3} = x_2 + x_1 + x_4 + x_5 \geq 1, \quad f_{2,4} = x_2 + x_3 + x_4 + x_5 \geq 1$$

- For NLP:

$$g_{2,1} = (1 - x_2)(1 - x_1)(1 - x_3)(1 - x_4) = 0,$$

$$g_{2,2} = (1 - x_2)(1 - x_1)(1 - x_3)(1 - x_5) = 0,$$

$$g_{2,3} = (1 - x_2)(1 - x_1)(1 - x_4)(1 - x_5) = 0,$$

$$g_{2,4} = (1 - x_2)(1 - x_3)(1 - x_4)(1 - x_5) = 0$$

Then the process is repeated for the rest of buses to make sure that each constraint has only three adjacent buses. Table 2.8 shows the limited channel capacity case results.

Table 2.8: Limited channel capacity case results

IEEE Test System	Number of Channels	Number of PMUs		Number of NLP Solutions
		MILP	NLP	
14-bus	3	4	4	1
57-bus	4	17	17	4
118-bus	6	32	32	3
300-bus	7	87	87	3

2.4.6 Remarks on OPP Problem Simulation Results

MILP and NLP comparison is conducted using different IEEE test case systems. Five case studies, which are Power flows, zero injections, limited communications, PMU failure, and limited PMU channels, are formulated using MILP and NLP approaches. A new formulation for zero injection using NLP is presented and examined. MATLAB's *intlinprog* function is used to solve the MILP, while NLP is solved by MATLAB's *fmincon* function with SQP solver. The initial values are chosen as random numbers in the feasible region. In a large-scale system, the initial values should be designed carefully to make the NLP converge to the minimum point. The total number of the initial values should not exceed 45% of total number of buses. Then some of the initial values can be designed with different random numbers to achieve several solutions. The nonlinear constraints tolerance can be varied from 10^{-4} to 10^{-12} to get the least number of PMUs. From Table 2.1, we can see that NLP obtains the least number of PMUs as same as MILP. NLP can also provide several solutions to the OPP problem. One of the NLP optimal sets matches the MILP solution. On the other hand, the computational time of the MILP is less than the NLP. Table 2.9 presents the average CPU time for both MILP and NLP on different IEEE systems. From Table 2.2 and Table 2.5, it can be seen that the number of PMUs in both methods is reduced to be less than the general case because of the power flow measurements and zero injection measurements, respectively. On the contrary, more PMUs are resulted in the restricted communication

and PMU failure cases as shown in Table 2.6 and Table 2.7. A backup set is generated for the single PMU failure case which would increase the PMU installation cost. It should be noted that the number of PMUs would be reduced if power flows and zero injections are considered in this case. To validate the effectiveness of the NLP zero injection formulation,

Table 2.9: MILP and NLP CPU time comparison

Case	IEEE Test System	CPU Time (s)	
		MILP	NLP
None	14-bus	0.0313	0.1563
	57-bus	0.0469	0.9375
	118-bus	0.0781	9.9063
	300-bus	0.0938	49.7656
Power Flow Measurements	14-bus	0.0313	0.0781
	57-bus	0.0469	0.4844
	118-bus	0.0625	6.7500
	300-bus	0.0938	43.3750
Zero Injection Measurements	14-bus	0.0313	0.0938
	57-bus	0.0469	0.8423
	118-bus	0.0781	6.7969
	300-bus	0.1094	43.2344
Limited Communication Facility	14-bus	0.0313	0.0781
	57-bus	0.0469	0.6406
	118-bus	0.0625	6.3906
	300-bus	0.0938	44.5469
Single PMU Failure	14-bus	0.0313	0.0781
	57-bus	0.0469	0.8438
	118-bus	0.0625	6.7969
	300-bus	0.0938	45.4063
Limited Channel Capacity	14-bus	0.0313	0.0938
	57-bus	0.0469	13.2188
	118-bus	0.0781	25.6875
	300-bus	0.1250	64.5313

a comparison of several algorithms results for zero injection case is shown in Table 2.10. For further analysis, the proposed zero injection formulations for MILP and NLP are evaluated on a large 2383-bus Polish system provided by MATPOWER [40] as can be seen from Table 2.11. Therefore, MILP and NLP approaches are effective to work out the OPP problem, and they can provide the same results.

Table 2.10: Comparison results of zero injection using different methods

Method	IEEE Test System		
	14-bus	57-bus	118-bus
ILP [2]	3	12	29
TS [16]	3	13	-
GA [14]	3	12	29
NSG [15]	-	-	29
PSO [17]	3	11	28
ILP [23]	3	13	29
SA [11]	3	11	-
ILP [22]	3	14	29
ILP [29]	3	11	28
ILP [31]	3	11	28
NLP [35]	3	13	29
Proposed MILP	3	11	28
Proposed NLP	3	11	28

Table 2.11: OPP results for a large 2383-bus Polish system

Case	Bus Location	Number of PMUs		Number of NLP Solutions	CPU Time (s)	
		MILP	NLP		MILP	NLP
None	—	746	746	8	0.9531	2.1607×10^3
Zero Injection Measurements	43,220,1185,1486 1871,2054,2086, 2196,2259,2285	740	740	7	1.0156	2.1393×10^3

2.5 Conclusion

Power grid observability modeling to tackle the OPP problem is presented using two approaches. MILP and NLP formulations for the OPP problem are demonstrated for complete observability. Nonlinear programming has an advantage of providing several optimal solutions compared to the MILP method. However, mixed integer linear programming has less CPU time compared to the nonlinear programming. MILP zero injection formulation is enhanced to solve the redundancy and optimality limitations. A new zero injection formulation for nonlinear programming is developed. Power flows, zero injections, limited communication facilities, PMU failure, and limited channel capacity case studies are demonstrated for the two methods. MILP and NLP advantages and disadvantages are discussed.

Chapter 3: PMU Measurements for Oscillation Monitoring: Connecting Prony Analysis with Observability

3.1 Introduction

Phasor measurement units (PMUs) installation can take several years to provide complete observability of the power grid. With the minimization techniques (e.g., MILP or NLP), the optimal PMU placement (Chapter 2) can be achieved. PMUs can be installed to the third or fifth of the system buses to ensure complete observability. In reality, power system can have a large amount of buses as the U.S. eastern interconnection which has around 70,000 buses. In this case, 14,000 to 24,000 PMUs are needed to make the system fully observable. According to the U.S. Department of Energy, the overall cost of PMU installation (including equipment, labor, communication, and security) is ranged from \$40,000 to \$180,000 [6]. Therefore, installing PMUs to make the system entirely observable is planned with stages and can take several years. Only 2500 PMUs are installed in the North American power grid (U.S. Department of Energy, 2018). In this chapter ², PMU measurements for oscillation monitoring are studied to provide the most observable bus which can better reflect the inter-area oscillation using Prony analysis. When a PMU is placed on the observable bus, the power system security is enhanced and the inter-area oscillation can be easily detected.

Phasor measurement units (PMUs) have been put into power grid for real-time monitoring. Using PMU data to identify electromechanical oscillations has been studied in the literature and an IEEE PES taskforce report [8] has been published in 2012. For ringdown

²This chapter was accepted for publication in IEEE Power and Energy Society General Meeting [41], 2019.

signals, or measurements captured for a transient event, Prony analysis and Eigensystem Realization Algorithm (ERA) are two measurement-based identification methods [9]. More specifically, Prony analysis has been introduced in power system oscillation mode estimation in 1980s by J. Hauer [42]. As an extension, Prony analysis based on multiple channel data was presented in [43]. In [44], multiple channel Prony analysis was formulated as a weighted least squares estimation problem with the weights obtained from single-channel Prony analysis. The estimation accuracy shows significant improvement.

Prony analysis accuracy also depends on the specification of system model order and sampling rate. Experiments have been conducted on Prony analysis to show the influence of model order and sampling rate on oscillation estimation accuracy [45]. The remarks on sampling rate influence on experiments in [45] are corroborated based on the analysis carried out in [46].

The objective of this chapter is to examine estimation accuracy of Prony analysis and relate the indicator of accuracy to the physical system dynamic analysis.

Prony analysis is essentially to solve a least squares estimation (LSE) problem notated as $Ha = Y$ where H is the Hankel matrix built upon measurements, Y is the measurement vector, and a is the parameter vector to be found. Since the solution of the overdetermined problem \hat{a} is determined by the normal equation: $\hat{a} = (H^T H)^{-1} H^T Y$, a larger conditional number of $H^T H$ (the ratio of the maximal singular value versus the minimum) indicates a worse estimation accuracy. In ERA, singular value decomposition (SVD) of Hankel matrices will be conducted to construct dynamic system matrices. The above information indicates that singular values of Hankel matrices can give indication regarding estimation accuracy. A paper in 2013, indeed relies on SVD of Hankel matrices to judge PMU placement for dynamic stability assessment [47].

To investigate how singular values of a Hankel matrix relate to a physical system model, dynamic modeled-based observability is used to rank measurements generated from a known

system model. The rank based on the observability will be shown to match the rank based on Hankel matrix singular values.

To this end, it is clear that the singular values of a Hankel matrix reflect signal observability of oscillation modes and hence they provide reasonable indication of estimation accuracy. Built upon this knowledge, the sensitivity of system model order assumption and noise level on estimation accuracy using the singular value plots is further studied.

The rest of the chapter is organized as follows. Section 3.2 gives a brief introduction on Prony analysis. Section 3.3 presents modal decomposition-based observability computation. Section 3.4 presents test case results using the two approaches: observability computing based on a known dynamic model and measurement-based Hankel matrix singular value computation. Section 3.5 concludes the chapter.

3.2 Prony Analysis

3.2.1 Prony Analysis Principle

Consider a Linear-Time Invariant (LTI) system with the initial state of $x(0) = x_0$, where $x \in \mathbb{R}^n$ is the stator variable column vector. The dynamic model can be expressed as the follows.

$$\dot{x}(t) = Ax(t) \quad (3.1)$$

$$y(t) = Cx(t) \quad (3.2)$$

where $y \in \mathbb{R}$ is a scalar output, $A \in \mathbb{R}^{n \times n}$ and $C \in \mathbb{R}^{1 \times n}$ are system dynamic and measurement matrices. The order of the system is n if A is full rank. Notation λ_i , p_i , and q_i represent the i -th eigenvalue, the corresponding right eigenvector, and the left eigenvector

of A respectively. The scalar output y can be represented as:

$$y(t) = \sum_{i=1}^n \underbrace{C(q_i^T x_0)}_{R_i} p_i e^{\lambda_i t}, \quad (3.3)$$

where R_i is named as a residual.

The observed or measured $y(t)$ consists of $N + 1$ samples which are equally spaced by Δt . The samples are notated as $y_k = y(t_k)$, $k = 1, \dots, N$. k th sample y_k can be written in the exponential form as:

$$y_k = y(t_k) = \sum_{i=1}^n R_i z_i^k, \quad k = 0, \dots, N, \quad (3.4)$$

where $z_i = e^{\lambda_i \Delta t}$, and z_i is the i th eigenvalue of the system in discrete time domain. z_1, z_2, \dots, z_n are the roots of the n -th characteristic polynomial function of the system:

$$z^n - (a_1 z^{n-1} + a_2 z^{n-2} + \dots + a_n z^0) = 0. \quad (3.5)$$

While the roots may be complex numbers, the system polynomial coefficients a_i are real numbers.

From (3.5), the linear prediction model can be obtained.

$$z^n = a_1 z^{n-1} + a_2 z^{n-2} + \dots + a_n z^0 \quad (3.6)$$

$$\Rightarrow y_n = a_1 y_{n-1} + a_2 y_{n-2} + \dots + a_n y_0 \quad (3.7)$$

A vector of the signal samples from step n to step N can be expressed as an overdetermined problem or LSE problem (3.8).

$$\underbrace{\begin{bmatrix} y_n \\ y_{n+1} \\ \vdots \\ y_N \end{bmatrix}}_Y = \underbrace{\begin{bmatrix} y_{n-1} & y_{n-2} & \cdots & y_0 \\ y_n & y_{n-1} & \cdots & y_1 \\ \vdots & \vdots & \ddots & \vdots \\ y_{N-1} & y_N & \cdots & y_{N-n} \end{bmatrix}}_H \underbrace{\begin{bmatrix} a_1 \\ a_2 \\ \vdots \\ a_n \end{bmatrix}}_a \quad (3.8)$$

H is a Hankel matrix of $(N + 1 - n) \times n$ dimension. The best estimate of a is found from the following normal equation.

$$\hat{a} = H^\dagger Y \quad (3.9)$$

where H^\dagger notates the Moore-Penrose pseudoinverse of H and $H^\dagger = (H^T H)^{-1} H^T$. The eigenvalues of the discrete system z_i can be found by seeking the roots of the polynomial (3.5). The eigenvalues of the continuous system λ_i can be found as $\frac{\log z_i}{\Delta t}$.

To find the residuals R_i , we examine (3.4). Eq. (3.4) can be expressed as another LSE, shown in (3.10).

$$\begin{bmatrix} z_1^0 & z_2^0 & \cdots & z_n^0 \\ z_1^1 & z_2^1 & \cdots & z_n^1 \\ \vdots & \vdots & \vdots & \vdots \\ z_1^N & z_2^N & \cdots & z_n^N \end{bmatrix} \begin{bmatrix} R_1 \\ R_2 \\ \vdots \\ R_n \end{bmatrix} = \begin{bmatrix} y_0 \\ y_1 \\ \vdots \\ y_N \end{bmatrix} \quad (3.10)$$

Solving (3.10) leads to the estimation of R_i . With this information, the signal can be reconstructed using (3.4).

3.2.2 Singular Value Decomposition of the Prony Analysis H Matrix

The SVD of the H matrix of the Prony analysis is the factorization of this matrix into the product of three matrices, and can be expressed as follows.

$$H = U\Sigma V^* \quad (3.11)$$

where the dimension of H is $(N - n + 1) \times n$, U is $(N - n + 1) \times (N - n + 1)$ matrix, Σ is $(N - n + 1) \times n$ diagonal matrix of positive real singular values of matrix H , and V^* is the conjugate transpose of V which is $n \times n$ matrix. U and V are unitary matrices, and the diagonal matrix Σ is given by the follows.

$$\Sigma = \begin{bmatrix} \Sigma_1 \\ 0 \end{bmatrix}, \quad n \leq (N - n + 1) \quad (3.12)$$

where Σ_1 is the diagonal of $\{\sigma_1, \sigma_2, \dots, \sigma_n\}$, and note that $\sigma_1 \geq \sigma_2 \geq \dots \geq \sigma_n$.

3.3 Modal Decomposition and Observability of Modes

The system matrix A has the following characteristic related to an eigenvalue λ_i :

$$Av_i = \lambda_i v_i \quad (3.13)$$

where v_i is right eigenvector associated with λ_i . Then (3.13) can be represented as the following:

$$A \underbrace{\begin{bmatrix} v_1, v_2, \dots, v_n \end{bmatrix}}_V = \begin{bmatrix} \lambda_1 v_1 & \lambda_2 v_2 & \dots & \lambda_n v_n \end{bmatrix} = V\Lambda \quad (3.14)$$

where V is the right eigenvector matrix and $\Lambda = \text{diag}\{\lambda_1, \dots, \lambda_n\}$. We may further find:

$$\Lambda = V^{-1}AV \quad (3.15)$$

$$A = V\Lambda V^{-1}. \quad (3.16)$$

The dynamic model can be expressed by the following:

$$\dot{x}(t) = V\Lambda V^{-1}x(t) \quad (3.17)$$

Define $\tilde{x} = V^{-1}x$ (or $x = V\tilde{x}$), then the dynamic system represented by \tilde{X} is as follows.

$$\begin{aligned} \dot{\tilde{x}}(t) &= \Lambda\tilde{x}(t), \text{ Or:} \\ \dot{\tilde{x}}_i(t) &= \lambda_i\tilde{x}_i(t) \end{aligned} \quad (3.18)$$

The time domain expression of every element of the new state vector \tilde{x} can be found independently with the i -th eigenvalue:

$$\tilde{x}_i(t) = e^{\lambda_i t} \tilde{x}_i(0) \quad (3.19)$$

The output of the system will be expressed as the following:

$$y(t) = CV\tilde{x}(t) = CV \begin{bmatrix} \tilde{x}_1(0)e^{\lambda_1 t} \\ \vdots \\ \tilde{x}_n(0)e^{\lambda_n t} \end{bmatrix} = \sum_{i=1}^n \Omega_i \tilde{x}_i(0) e^{\lambda_i t} \quad (3.20)$$

where $\Omega = CV$ is the observability row vector corresponding to each eigenvalue.

From the output or measurement expression $y(t)$, it can be seen that for the same initial condition notated by $x(0)$ and further $\tilde{x}(0)$, different measurements will have different

observability of each eigenvalue. Thus, Ω will be computed for measurements and $|\Omega_i|$ will be used to rank the measurements based on their observability to the i -th eigenvalue.

3.4 Case Studies

The two approaches for measurement ranking will be applied to two systems: the 2-area 4-machine case and the 16-machine 68-bus system. The measurement data are generated using the power system toolbox (PST) [48]. PST also has the capability to conduct small-signal perturbation and give the linear system matrices. The observability vectors are computed based on the system matrices obtained. Though MATLAB's signal processing toolbox has a Prony analysis function that can give a discrete system transfer function from a given time-series signal, it does not provide the intermediate information regarding Hankel matrix. As such, a Prony analysis toolbox developed for [44, 49] is utilized to conduct Prony analysis, including least squares estimation to find coefficient vector a , eigenvalue computing, and signal reconstruction.

3.4.1 Two-Area Four-Machine System

The classic two-area four machine system for inter-area oscillation study (shown in Fig. 3.1) is used for the first case study. The four generators are assumed to have a second-order swing dynamics each. Twenty seconds simulation is conducted for a short-circuit transient event. The measurements are resampled to have equal time steps.

3.4.1.1 Comparison of Different Signals

The sampling rate is chosen to be 0.03 s. Three voltage signals for three different buses (buses 1, 13, and 101) are selected. Research in [50] has a given detailed analysis on interarea oscillation observability for buses on a radial path. It is found that the bus located in the middle of the path is shown to have the best observability. In turn, Bus 101 is expected to

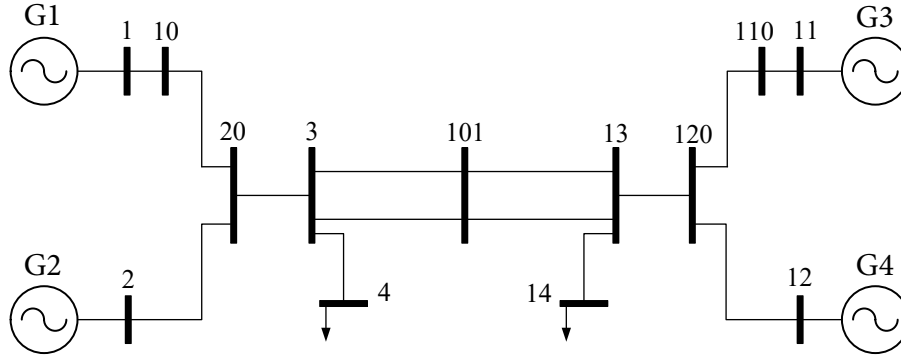


Figure 3.1: The two-area four machine test case in PST.

Table 3.1: The observability approach of buses 1, 13, and 101 with damping ratio and frequency of the 13-bus system

Mode	Observability			Damping Ratio	Frequency (Hz)
	Bus 1	Bus 13	Bus 101		
1	0.04	0.02	0.11	0.00	0.56
2	0.05	0.04	0.04	-0.00	1.20
3	0.03	0.05	0.06	0.00	1.21

have the largest absolute value for its observability corresponding to the inter-area oscillation mode.

This is confirmed by the observability analysis conducted base on the linear system matrices. The observability along with the damping ratio, and frequency of the system modes are also presented in Table 3.1. In this system, three oscillation modes are identified and shown in Table 3.1: 0.56 Hz inter-area oscillation mode and two local oscillation modes at 1.20 Hz and 1.21 Hz. We can see clearly that Bus 101 has a larger observability on the 0.56 Hz mode than the other two buses.

It is known that the angle difference between the buses located in two areas should better reflect inter-area oscillations compared to the angle difference between two buses located in the same area. In addition to the three voltage signals, three angle difference signals are also

selected: $\theta_2 - \theta_1$, $\theta_{11} - \theta_1$, and $\theta_{11} - \theta_{12}$. Since PST does not give the measurement matrix on the bus angles, the observability for angle differences is omitted.

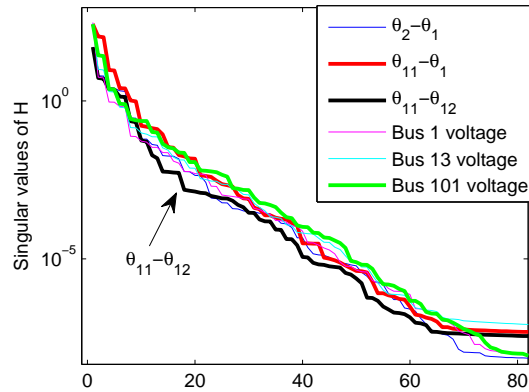


Figure 3.2: Singular values for the Hankel matrices related to the six signals. The system order is 220.

The Hankel matrices H of the six selected signals are built based on the simulation data. Fig. 3.2 shows the singular values of the H matrices of the three voltage signals and the three angle signals. It can be clearly seen that the singular values related to Bus 101 (in the middle of the path) and the angle difference of buses in two areas ($\theta_{11} - \theta_1$) have singular values on the top. On the other hand, angle difference for two buses located in one area ($\theta_{11} - \theta_{12}$) is on the bottom of the chart. The singular value plots confirm that Bus 101's voltage magnitude and the angle between two areas have the best observability of interarea oscillation mode. Fig. 3.3 presents the reconstructed signals against the original measurements (thin blue lines).

3.4.1.2 Comparison of Model Order Assumption

For the angle difference signal ($\theta_{11} - \theta_{12}$) related to two buses in Area 2, Prony analysis with different model order assumptions are carried out. The model order is assumed to be 50, 120 and 220, respectively. The singular value plots of the corresponding Hankel matrices are shown in Fig. 3.4.

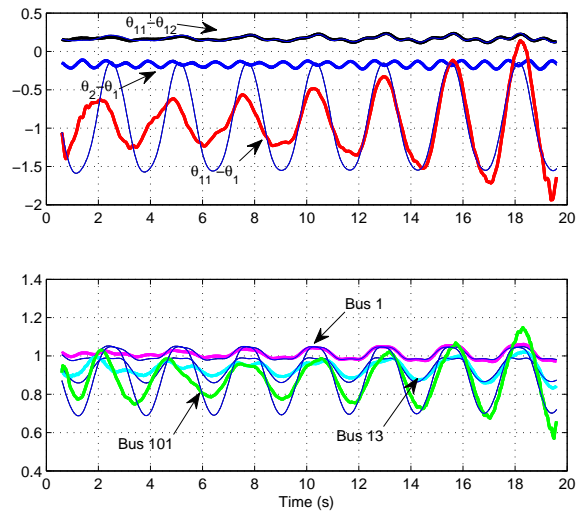


Figure 3.3: Comparison of the reconstructed signals against the original measurements (thin blue lines).

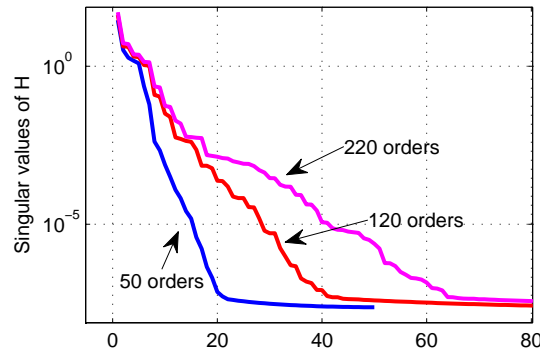


Figure 3.4: Singular values for the Hankel matrices related to three orders: 50, 120 and 220.

The singular value plots clearly show that high-order results in better estimation accuracy. This point has been recognized generally (see [51] Chapter 10). The reconstructed signals are presented in Fig. 3.5. It can be seen that high order assumption results in better match between the reconstructed signal and the original signal.

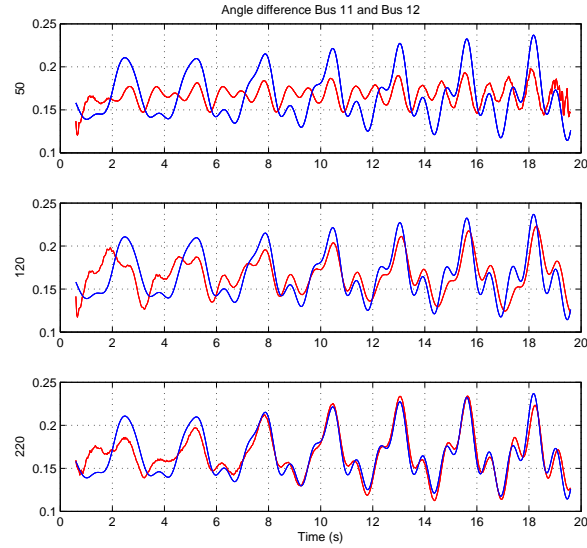


Figure 3.5: Comparison of the reconstructed signals against the original measurements for different model order assumptions. Blue lines are the original measurements while the red lines are the reconstructed signals.

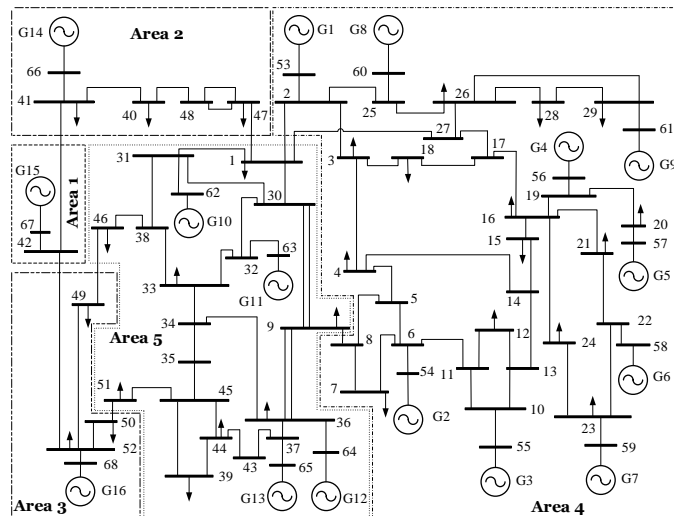


Figure 3.6: 16-machine, 68-bus test case.

3.4.2 16-Machine 68-Bus System

A larger power system, which is the 16-machine, 68-bus system, is used to further validate that both of the observability calculation and Prony analysis singular value examination lead to the same findings. This system is a reduced model of the New England Test System

(NETS)-New York Power System (NYPS) interconnected system [52] and has five areas. NETS is represented by area 4 which has generators G1 to G9, while NYPS is represented by area 5 which has generators G10 to G13 as shown in Fig. 3.6 [52]. The other three areas have equivalent generators G14 to G16.

Three voltage signals in different areas are chosen: Bus 5, Bus 29, and Bus 67. Their observability related to four modes with lowest frequencies are computed and the results are shown in Fig. 3.7. From this figure, it can be seen that Bus 29 is more observable compared to Bus 5 and Bus 67 for the four modes. Among the four modes, modes 1 and 3 are identified as inter-area oscillation modes, with their mode shape and participation factors shown in Fig. 3.8.

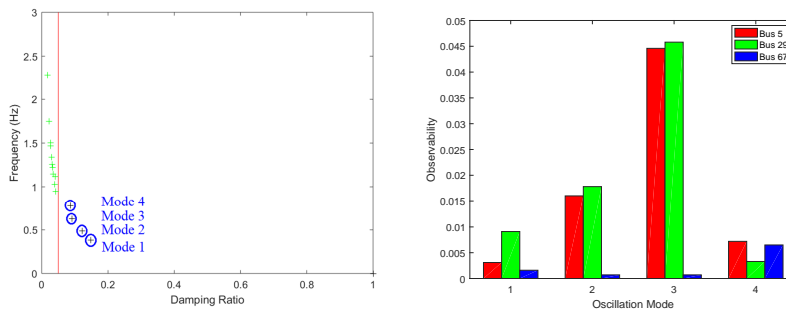


Figure 3.7: Observability of different buses. (a)Four low-frequency modes. (b)Buses 5, 29, and 67 observability of the four indicated modes.

The simulation data generated by PST is used for Prony analysis. The system order is set to be $n = 150$, and the sampling rate is defined to be 0.03 s. The singular values of the Hankel matrix H of buses 5, 29, and 67 are shown in Fig. 3.9. The singular value plots show that Bus 29 will result in best estimation accuracy. This finding corroborates with that from the observability shown in Fig. 3.7.

The reconstructed signals are presented in Fig. 3.10. It can be seen that the match of Bus 29 is better compared to that of Bus 5.

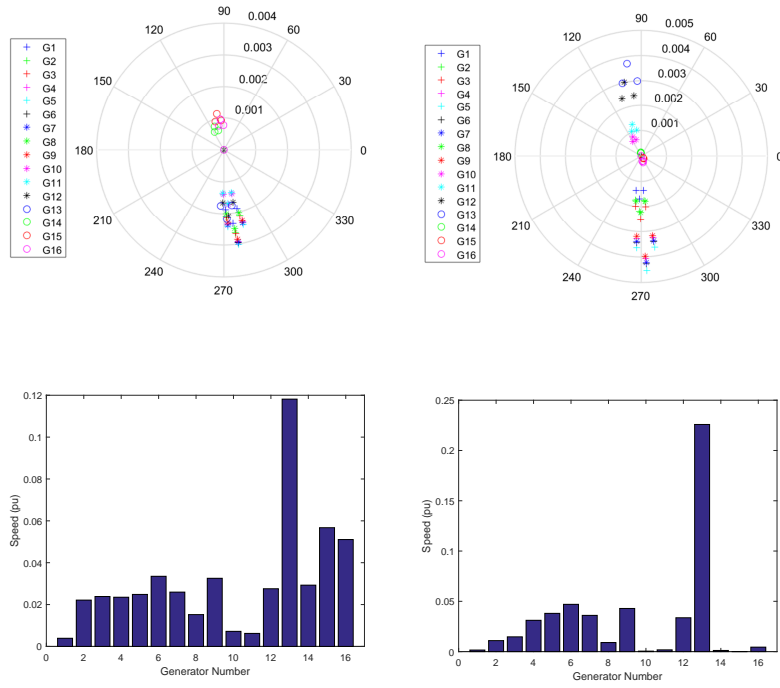


Figure 3.8: Oscillation modes 1 and 3 participation factor of the 68-bus system. (a)Compass plot of rotor speed of mode 1 and (b)mode 3. (c)Real part of speed participation factor of mode 1 and (d)mode 3.

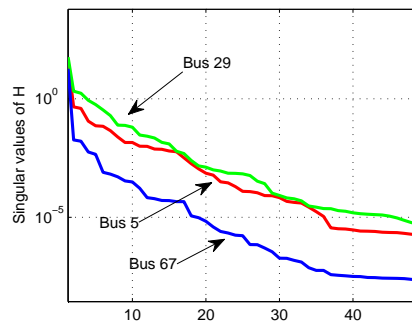


Figure 3.9: Singular values of the Hankel matrix corresponding to bus voltage measurement at 5, 29, and 67.

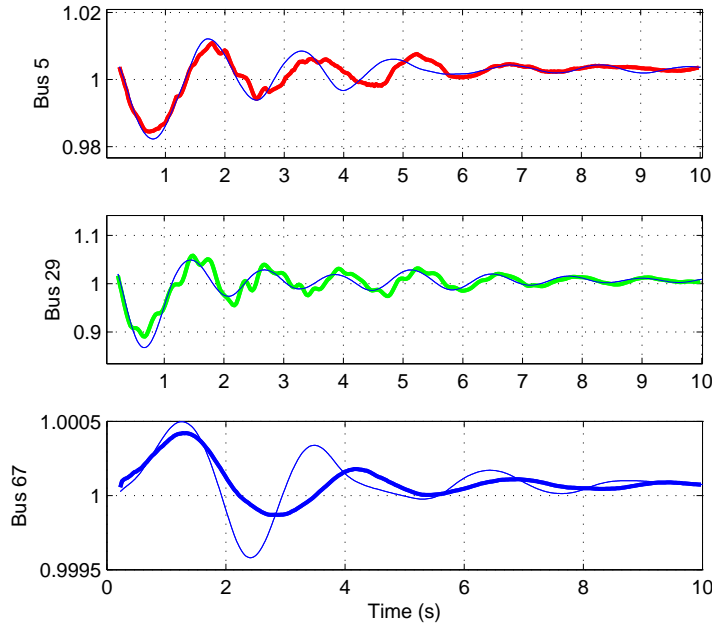


Figure 3.10: Comparison of the reconstructed signals against the original measurements. Blue lines are the original measurements.

3.4.2.1 Sensitivity Analysis of Noise Level

Bus 29's voltage measurement is polluted with uniformly distributed random noise. The singular value plots are generated (shown in Fig. 3.11) for the measurement with noise at signal noise ratio (SNR) of 80 dB, 40 dB, and 20 dB. Note that PMU data usually has a SNR at 40 dB [53]. It can be clearly seen that large noise leads to inaccurate estimation.

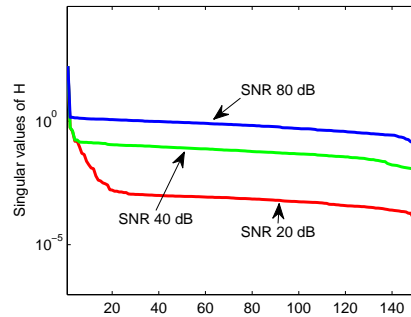


Figure 3.11: Singular values of the Hankel matrix for different noise levels.

3.5 Conclusion

This chapter demonstrates that the singular values of the Hankel matrix built for Prony analysis or ERA can serve as an indicator for estimation accuracy. Signals with large observability also show large singular values. In addition, influence of model order and noise level can also be demonstrated by the singular values. Two test cases, which are the two-area four-machine and the 16-machine 68-bus systems, are used to illustrate the relationship between singular values and dominant oscillation mode observability.

Chapter 4: Measurement-Based Eigenvalue Identification Using Prony Analysis, Matrix Pencil and Eigensystem Realization Algorithm

4.1 Introduction

In addition to rank the PMU measurements for oscillation monitoring, the PMU data can play an important role to detect the inter-area oscillation modes. Conventionally, the oscillation modes in power system are analyzed with offline modal analysis method. Therefore, the eigenvalues are identified with a linearized differential algebraic equation (DAE) model with a specific equivalent point [54]. In other words, the results will be related to that equivalent point. In reality, the operating conditions of the system are changing frequently. The real power system cannot be predicted accurately, and offline modal analysis would not help to detect the inter-area modes. Hence, measurement based-methods with PMU data are investigated in this chapter ³ to provide a real time monitoring and oscillation detection with the current state of the power system. Wide Area Measurement System (WAMS) is responsible to collect the synchronized measurements from PMUs with time tags from GPS. Then the PMU data are sent to the Phasor Data Concentrator (PDC). Oscillation Monitoring System (OMS) is built to the PDCs to detect the oscillation modes with the measurement-based algorithms [56]. Based on the eigenvalue analysis, the frequency and the damping ratio can be identified. Inter-area oscillation mode can be observed with low frequencies at 0.1 to 1 Hz, and the associated damping ratio range is between 0 and 17% in most cases.

Using measurement data, e.g., synchrophasors from Phasor Measurement Units (PMUs), to find out system dynamic information is of practical interest [53]. The measurement data

³This chapter was submitted to International Transactions on Electrical Energy Systems [55], 2019.

are classified into three categories which are ambient, probing, and ringdown. Ambient data are related the variation of generators and loads at a fixed operating condition. Probing data are the study of injected low-level pseudo-random noise to test the system performance. Ringdown data occur when a large disturbance is observed in the system. For probing and ambient data, several techniques have been studied in the literature. Autoregressive model (AR), autoregressive moving average model (ARMA), and autoregressive moving average exogenous (ARMAX) with a recursive least square (RLS) are presented in [57–59]. With RLS, some of those methods can be applied to ringdown data. However, their computation time is significant in case of a large power system and they are sensitive to the model order [8]. Consequently, the inter-area oscillation cannot be accurately identified since different model orders affect the accuracy of the modes detection.

In addition, mode-meter analysis method for ambient data using Yule-Walker (YW) algorithm is introduced in [60]. Performance of three different mode-meter algorithms based on YW and subspace system identification is presented in [61]. Those methods can be applied only to ambient data. Nevertheless, complex analysis is needed for large power systems, and accurate estimation cannot be achieved with very noisy signals [61]. Nonlinear and non-stationary analysis using Hilbert spectral analysis (HSA) is presented in [62, 63]. However, this algorithm cannot provide an accurate estimation of two separated modes when frequency or damping ratio difference is small [64].

Moreover, Prony analysis, Matrix Pencil (MP), and Eigensystem Realization Algorithm (ERA) are the three major linear system identification methods for ringdown signals captured for transient events [8]. As mentioned in Chapter 3, Prony analysis was introduced to the power system oscillation mode estimation by J. Hauer [42]. As an extension, Prony analysis based on multiple channel data was presented in [43]. In [44], multiple channel Prony analysis was formulated as a weighted least squares estimation problem with the weights obtained from single-channel Prony analysis. Prony analysis has been shown to have difficulty

extracting modes with reduced-order model. Eigensystem Realization Algorithm (ERA) for parameter identification and model reduction of dynamical systems was introduced in 1985 [65] relying on system realization theory introduced by Gilbert [66] and Kalman [67]. Applying ERA in power systems to find low-order models from time-domain simulation data has been investigated in [9]. However, ERA approach may not provide an accurate signal reconstruction with low orders. Further, using MP to estimate dynamic system eigenvalues for an electromagnetic transient response was presented in [68,69]. This method was applied to the power systems in 2005 to estimate dominant oscillation modes from Western Electricity Coordinating Council (WECC) frequency responses of 6 seconds [70]. In [71], MP and Prony analysis are compared for their capabilities of modal extraction of noisy power system signals. MP has been proven to be more capable of mode extraction than Prony analysis.

In this chapter, the identification of the system dynamic information using PMU data is investigated. Based on the literature, methods such as AR, ARMA, ARMAX, YW, and Prony analysis to identify the inter-area oscillation modes are either sensitive to model orders or noise signals. An alternative approach is to directly identify a reduced-order model based on measurements. With real-world PMU measurements more accessible, this approach will generate high practical interest. MP and ERA methods can identify the dynamic model based on a reduced order model assumption. Those two methods are studied and the key technique of noise resiliency and model order insensitivity as singular value decomposition (SVD)-based rank reduction is identified. A reduced-order Prony analysis method through Hankel matrix rank reduction is proposed in this chapter. The new Prony analysis can accurately identify system eigenvalues from noisy signals. This proposed Prony method has an excellent performance with different model orders. In addition, an improved ERA method based on SVD rank reduction technique is presented. The proposed ERA can handle multiple signals and provide accurate eigenvalues of the reduced-order model compared to similar methods in the literature.

All three methods (Prony analysis, MP, and ERA) form Hankel matrices from measurement data. In Prony analysis, a single Hankel matrix is formed, where eigenvalues are found by identifying the real coefficients from the polynomial characteristic equation through least square estimation (LSE). In MP and ERA, shifted Hankel matrices are formed in respective approach and the relation between the two matrices are explored. In MP, the two matrices are related with system eigenvalues and a generalized eigenvalue problem is formed [65]. In ERA, the two shifted Hankel matrices are related with system matrix A to find the eigenvalues.

While the 2012 IEEE PES taskforce report [8] offers a great guideline on the three methods, a thorough examination on their principles, multiple data handling, noise resilient techniques, and applications in large-scale power grid dynamics and real-world oscillation events is of great importance. This chapter achieves the aforementioned goals and the contribution is three-fold.

- First, this chapter has shed insight on the three major methods for eigenvalue identification applied to the power systems and identified the key technique of noise resilience as singular value decomposition (SVD)-based rank reduction. SVD-based rank reduction technique has been implemented in MP and achieved system order reduction and noise resilience [69, 72]. This technique is implemented in ERA for one of the Hankel matrices [8]. In this chapter, the rank reduction technique is further implemented on the second Hankel matrix of ERA to achieve a superior performance.
- Second, Prony analysis method to achieve reduced-order system eigenvalue identification and noise resilience is innovated. Prony analysis is known to be sensitive to system order assumptions. If the system order is assumed to be low, the reconstructed signal based on the identified eigenvalues poorly matches the original signal, especially for noisy signals. In this chapter, two techniques are employed, namely, Hankel matrix

rank reduction and eigenvalue reduction. The reduced-order Prony analysis method gives comparable performance as MP and ERA.

- Third, two case studies, including an RLC circuit example and a large-scale power grid oscillation example, clearly demonstrate the effectiveness of the three methods. Further, the capability of the proposed methods is validated by analyzing real-world oscillation events provided by Independent System Operator-New England (ISO-NE).

The remaining sections are organized as follows. Section 4.2 presents the principles of the three methods. Section 4.3 proceeds to the model reduction techniques used in the literature for MP and the innovation of Prony analysis improvement using Hankel matrix rank reduction technique. Section 4.4 presents the case studies. Section 4.5 concludes the chapter.

4.2 Principles of the Three Methods

4.2.1 Prony Analysis

Prony analysis principle is discussed in Chapter 3 (Section 3.2). Incorporating multiple measurement data has been introduced in [43]. Consider that the power system data has K channels which are obtained from the same period of time. For k -th channel ($k = 1, \dots, K$), the H matrix and Y vector can be formulated for every channel of the given data and notated as $H^{(k)}$ and $Y^{(k)}$. Then the a vector can be obtained by solving the following estimation problem.

$$\begin{aligned} & \left[(H^{(1)})^T \quad (H^{(2)})^T \quad \dots \quad (H^{(K)})^T \right]^T a \\ & = \left[(Y^{(1)})^T \quad (Y^{(2)})^T \quad \dots \quad (Y^{(K)})^T \right]^T \end{aligned} \quad (4.1)$$

where the superscript T notates transpose.

4.2.2 Matrix Pencil

Consider a single measurement output, in MP, two shifted Hankel matrices H_1 and H_2 are used. A Hankel matrix is formed in (4.2). Deleting the last row results in H_1 while deleting the first row results in H_2 . Both matrices are of dimension $(L + 1) \times (N - L)$.

$$H = \begin{bmatrix} y_0 & y_1 & \cdots & y_{N-L-1} \\ y_1 & y_2 & \cdots & y_{N-L} \\ \vdots & \vdots & \ddots & \vdots \\ y_L & y_{L+1} & \cdots & y_{N-1} \\ y_{L+1} & y_{L+2} & \cdots & y_N \end{bmatrix}_{(L+2) \times (N-L)} \quad (4.2)$$

$$H_1 = H(1 : L + 1, :) \quad (4.3)$$

$$H_2 = H(2 : L + 2, :) \quad (4.4)$$

H_1 can be decomposed and expressed as follows.

$$H_1 = P\beta Q \quad (4.5)$$

where $P \in \mathbb{R}^{(L+1) \times n}$, $\beta \in \mathbb{R}^{n \times n}$, and $Q \in \mathbb{R}^{n \times (N-L)}$.

P , Q , and β are defined as follows.

$$P = \begin{bmatrix} 1 & 1 & \cdots & 1 \\ z_1 & z_2 & \cdots & z_n \\ \vdots & \vdots & & \vdots \\ z_1^L & z_2^L & \cdots & z_n^L \end{bmatrix}, Q = \begin{bmatrix} 1 & z_1 & \cdots & z_1^{N-L-1} \\ 1 & z_2 & \cdots & z_2^{N-L-1} \\ \vdots & \vdots & & \vdots \\ 1 & z_n & \cdots & z_n^{N-L-1} \end{bmatrix}, \quad (4.6)$$

$$\beta = \text{diag}([R_1, R_2, \cdots, R_n]).$$

H_2 can be expressed as:

$$H_2 = PZ_0\beta Q \quad (4.7)$$

where Z_0 is a diagonal matrix:

$$Z_0 = \text{diag}([z_1, z_2, \dots, z_n]). \quad (4.8)$$

A generalized eigenvalue problem can be formulated based on the two shifted Hankel matrices. The eigenvalue z that can make $zH_1 - H_2$ to have a rank less than n must be one of the system eigenvalues z_i . This point can be proven by the following.

$$zH_1 - H_2 = zP\beta Q - PZ_0\beta Q = P(zI - Z_0)\beta Q. \quad (4.9)$$

Hence, if $z = z_i$, $zH_1 - H_2$ will have a rank less than n . Thus, z can be found by solving an ordinary eigenvalue problem:

$$zI - H_1^\dagger H_2. \quad (4.10)$$

Since H_1 and H_2 are Hankel matrices with rank n , SVD-based rank reduction can be performed on the two matrices. The rank reduction makes the eigenvalue identification robust against noise.

4.2.2.1 SVD-Based Rank Reduction

SVD-based rank reduction is briefly described here. A thin matrix $A \in \mathbb{R}^{M \times N}$ with rank of N can be decomposed as the follows.

$$A = U_A S_A V_A^T \quad (4.11)$$

where $U_A \in \mathbb{R}^{M \times M}$ and $V_A \in \mathbb{R}^{N \times N}$ are two unitary matrices. $S_A \in \mathbb{R}^{M \times N}$ is a diagonal matrix with singular values of A ($\sigma_{A1} \geq \sigma_{A2} \cdots \geq \sigma_N \geq 0$) as diagonal components. The rank reduction technique can be applied to (4.11) as follows.

$$A = \begin{bmatrix} U_{A1} & U_{A2} \end{bmatrix} \begin{bmatrix} S_{A1} & 0 \\ 0 & S_{A2} \end{bmatrix} \begin{bmatrix} V_{A1} & V_{A2} \end{bmatrix}^T \quad (4.12)$$

where $U_{A1} \in \mathbb{R}^{M \times n}$, $U_{A2} \in \mathbb{R}^{M \times (M-n)}$, $S_{A1} \in \mathbb{R}^{n \times n}$, $S_{A2} \in \mathbb{R}^{(M-n) \times (N-n)}$, $V_{A1} \in \mathbb{R}^{N \times n}$ and $V_{A2} \in \mathbb{R}^{N \times (N-n)}$. The reduced rank matrix A' is obtained as the following:

$$A \approx A' = U_{A1} S_{A1} V_{A1}^T \quad (4.13)$$

where A' has the same dimension of A . However, its rank is reduced to n .

SVD-based rank reduction can be applied to the Hankel matrix H in (4.2). The Hankel matrix is now expressed as follow.

$$H_{(L+2) \times (N-L)} = U S V^T \quad (4.14)$$

where $U \in \mathbb{R}^{(L+2) \times n}$, $S \in \mathbb{R}^{n \times n}$, $V \in \mathbb{R}^{(N-L) \times n}$. The two shifted Hankel matrices can be expressed as follows.

$$H_1 = U_1 S V^T \quad (4.15)$$

$$H_2 = U_2 S V^T \quad (4.16)$$

where U_1 is the first $(L + 1)$ rows of U and U_2 is the last $(L + 1)$ rows of U .

Equation (4.9) can be expressed as follows.

$$zH_1 - H_2 = (zU_1 - U_2)SV^T. \quad (4.17)$$

Hence, z_i can be found as the eigenvalues of $U_1^\dagger U_2$.

4.2.2.2 Multiple Channel Consideration

Multiple channel handling technique is introduced in [73]. For each channel, two shifted Hankel matrices will be formed. Notate $H_1^{(k)}$ and $H_2^{(k)}$ as the Hankel matrices based on channel k . The aggregated Hankel matrices are as follows.

$$H_1 = \begin{bmatrix} H_1^{(1)} & H_1^{(2)} & \dots & H_1^{(K)} \end{bmatrix} \quad (4.18)$$

$$H_2 = \begin{bmatrix} H_2^{(1)} & H_2^{(2)} & \dots & H_2^{(K)} \end{bmatrix} \quad (4.19)$$

The two Hankel matrices can be decomposed in the similar aforementioned way.

$$H_1 = P\beta Q \quad (4.20)$$

$$H_2 = PZ_0\beta Q \quad (4.21)$$

where P and Z_0 are defined the same as those in (4.6) and (4.8). β and Q are defined as the aggregated ones. Consider $\beta^{(k)}$ and $Q^{(k)}$ as those formed based on k -th channel. Then the aggregated matrices are as follows.

$$\beta = \begin{bmatrix} \beta^{(1)} & \beta^{(2)} & \dots & \beta^{(K)} \end{bmatrix} \quad (4.22)$$

$$Q = \text{diag}([Q^{(1)}, Q^{(2)}, \dots, Q^{(K)}]). \quad (4.23)$$

The system roots z_i can be obtained as the generalized eigenvalues that make the following matrix rank less than n :

$$zH_1 - H_2 \quad (4.24)$$

Similarly, SVD rank reduction can be applied to H_1 and H_2 . Based on those rank-reduced matrices, the eigenvalues will be found.

4.2.3 Eigensystem Realization Algorithm

Eigensystem realization algorithm (ERA) assumes that the dynamic response is due to an impulse input [8]. Consider a Linear-Time Invariant (LTI) system in discrete domain as the following:

$$x_{k+1} = Ax_k + Bu_k, y_k = Cx_k + Du_k \quad (4.25)$$

where $y \in \mathbb{R}^{K \times 1}$ is defined as the output column vector of the system with K output channels, $A \in \mathbb{R}^{n \times n}$, $B \in \mathbb{R}^{n \times 1}$, $C \in \mathbb{R}^{K \times n}$, and $D \in \mathbb{R}^{K \times 1}$ are system matrices. Assuming $x_0 = 0$, the system response due to an impulse input ($u_0 = 1, u_k = 0, k > 0$) can be found as follows.

$$\begin{aligned} x_0 &= 0, & y_0 &= D \\ x_1 &= B, & y_1 &= CB \\ x_2 &= AB, & y_2 &= CAB \\ &\dots & & \\ x_k &= A^{k-1}B, & y_k &= CA^{k-1}B \end{aligned} \quad (4.26)$$

Two shifted Hankel matrices are formed as follows.

$$\begin{aligned}
 H_1 &= \begin{bmatrix} y_1 & y_2 & \cdots & y_L \\ y_2 & y_3 & \cdots & y_{L+1} \\ \vdots & \vdots & \ddots & \vdots \\ y_{N-L+1} & y_{N-L+2} & \cdots & y_N \end{bmatrix}_{K(N-L+1) \times L} \\
 H_2 &= \begin{bmatrix} y_2 & y_3 & \cdots & y_{L+1} \\ y_3 & y_4 & \cdots & y_{L+2} \\ \vdots & \vdots & \ddots & \vdots \\ y_{N-L+2} & y_{N-L+3} & \cdots & y_{N+1} \end{bmatrix}_{K(N-L+1) \times L}
 \end{aligned} \tag{4.27}$$

It can be seen that the Hankel matrices can be decomposed as follows.

$$H_1 = \begin{bmatrix} CB & CAB & \cdots & CA^{L-1}B \\ CAB & CA^2B & \cdots & CA^L B \\ \vdots & \vdots & \ddots & \vdots \\ CA^{N-L}B & CA^{N-L+1}B & \cdots & CA^{N-1}B \end{bmatrix} \tag{4.28}$$

$$= \underbrace{\begin{bmatrix} C \\ CA \\ \vdots \\ CA^{N-L} \end{bmatrix}}_{\mathcal{O}} \underbrace{\begin{bmatrix} B & AB & \cdots & A^{L-1}B \end{bmatrix}}_{\mathcal{C}} \tag{4.29}$$

$$H_2 = \mathcal{O} \mathcal{A} \mathcal{C} \tag{4.30}$$

where \mathcal{O} is the observability matrix and \mathcal{C} is the controllability matrix.

Note that the two matrices are of the following dimensions:

$$\mathcal{O} \in \mathbb{R}^{K(N-L+1) \times n}$$

$$\mathcal{C} \in \mathbb{R}^{n \times L}$$

ERA employs SVD and further rank reduction to find two matrices to realize \mathcal{O} and \mathcal{C} . First, SVD is conducted for H_1 and the resulting matrices are marked with their dimensions as follows.

$$H_1 = USV^T,$$

where $U \in \mathbb{R}^{K(N-L+1) \times K(N-L+1)},$ (4.31)

$$S \in \mathbb{R}^{K(N-L+1) \times L}, V \in \mathbb{R}^{L \times L}$$

Only n components of $diag(S)$ will be kept to construct the reduced-rank Hankel matrix H'_1 .

$$H'_1 = \underbrace{U(:, 1:n)}_{U'} \underbrace{S(1:n, 1:n)}_{S'} \underbrace{(V(:, 1:n))^T}_{V'}$$

$$U' \in \mathbb{R}^{K(N-L+1) \times n},$$
 (4.32)
$$S' \in \mathbb{R}^{n \times n}, V' \in \mathbb{R}^{L \times n}$$

Similarly, rank reduction may also be applied to H_2 to have a low-rank Hankel matrix H'_2 . It is worth to mention that this step on H_2 rank reduction is not used in [8]. Rank reduction for H_2 leads to a superior performance as demonstrated in the case studies in Section 4.4. From the reduced-rank Hankel matrix, the observability and controllability matrices can be realized as follows.

$$\mathcal{O} = U' S'^{\frac{1}{2}}, \quad \mathcal{C} = S'^{\frac{1}{2}} (V')^T$$
 (4.33)

Thus, the system matrix A can be realized through the use of (4.30).

$$A = S'^{-\frac{1}{2}} U'^T H'_2 V' S'^{-\frac{1}{2}} \quad (4.34)$$

From A , eigenvalues of the discrete system can be found.

4.3 Order Reduction Techniques

The objective is to obtain eigenvalues of a low-order system. SVD rank reduction has been employed in MP and the order of the system can be specified. Performance of MP is excellent in terms of noise handling. One reason is that SVD-based reduction rules out many small singular values which are related to noise. With this procedure, MP is shown to have a better performance over Prony analysis [69]. This point is also validated for power system oscillation studies in [71].

In this section, we explore SVD rank reduction technique to improve the performance of Prony analysis.

In [69], Hankel matrix rank reduction is suggested for Prony analysis to better handle noise. On the other hand, the dimension of the Hankel matrix is the same even if the rank reduction was applied. In the following, an RLC circuit example is presented to first illustrate the effect on eigenvalue distribution with Hankel matrix rank reduction. As a consequence of rank reduction, distribution of eigenvalues has a radical change. The dominant eigenvalues and the non-dominant eigenvalues become clearly separated. With this effect, the non-dominant eigenvalues are further eliminated. Thus, a low-order system is identified.

A series RLC circuit shown in Fig. 4.1 is used as an illustrative example. A step change in the source voltage is applied at $t = 0$ second, the current and the capacitor voltage are chosen as the measurement. The current i and voltage V_c in Laplace domain are expressed as follows.

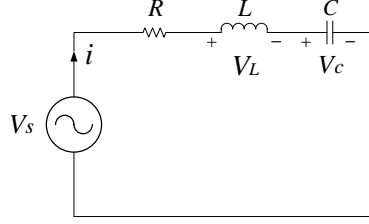


Figure 4.1: RLC circuit.

$$i = \frac{C}{LCs^2 + RCs + 1} \quad (4.35)$$

$$V_c = \frac{1}{s(LCs^2 + RCs + 1)}$$

Obviously, the two signals have different number of eigenvalues. The current has two poles: $\lambda \approx -\frac{R}{2L} \pm j\frac{1}{\sqrt{LC}}$. The voltage has these two poles and an additional pole as 0.

The sampling rate is 0.001 s for the measurement data. The number of samples in 0.1 seconds is 101 ($N = 101$). The system is assumed to have an order of 33. As a result, the Hankel matrix dimension is 68×33 . As a comparison, order 3 is assumed for another case. The resulting Hankel matrix has a dimension of 98×3 . For each order assumption, signals with and without noise (0.3 pu uniformly distributed) are examined. Fig. 4.2 presents the two cases when order is assumed as 33 and Fig. 4.3 presents the two cases when the order is assumed as 3.

It can be seen that when the signals have no noise pollution, Prony analysis with different order assumptions correctly reflect eigenvalues (Figs. 4.2a and 4.3a). The reconstructed signals match the original signals well. From Fig. 4.2a, it can also be observed that if the Hankel matrix has a low rank, the resulting identified eigenvalues distribute on the real and imaginary space with an obvious pattern. The system modes $(0, -37.7 \pm j2\pi37.47)$ are clearly separated from the other modes.

When the signals are polluted with noise (Figs. 4.2b and 4.3b), it can be seen that the reconstructed signals match the original ones well when the order is assumed high. If a

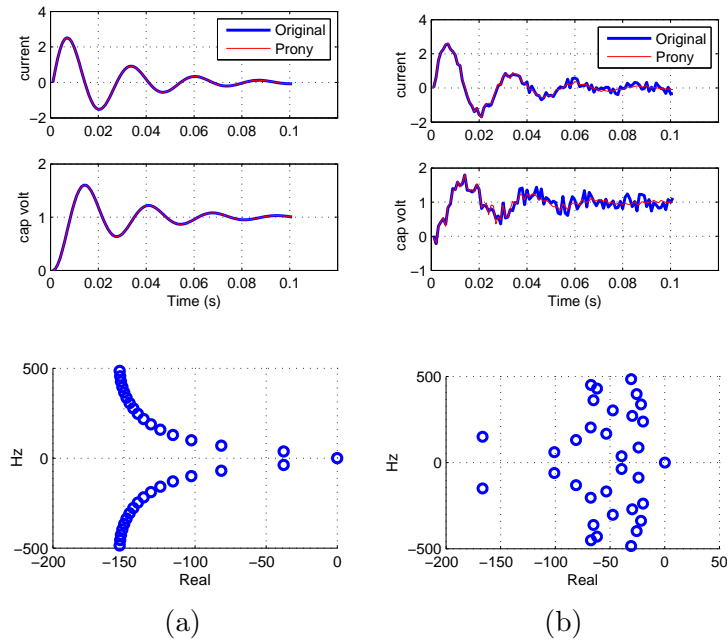


Figure 4.2: RLC circuit reconstructed signals and estimated eigenvalues with assumed order of 33. (4.2a) without noise. (4.2b) with noise.

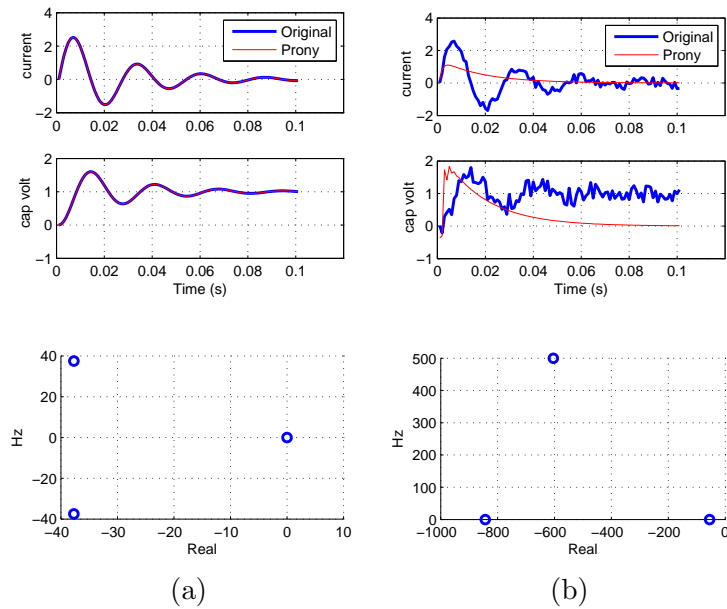


Figure 4.3: RLC circuit reconstructed signals and estimated eigenvalues with assumed order of 3. (4.3a) without noise. (4.3b) with noise.

low order is assumed, the match is poor. In addition, when there is noise, the eigenvalues identified for the 33 order system no longer have a clear pattern. The 37 Hz LC resonance mode is located more towards the left half-plane (LHP) compared to several other modes.

We now show the effect of rank reduction on the Hankel matrix. Using the same noise polluted signals shown in Fig. 4.2b and applying rank reduction on the corresponding 68×33 Hankel matrix, the resulting rank-3 Hankel matrix leads to system eigenvalues (shown in Fig. 4.4a) with a similar pattern as that shown in Fig. 4.2a. The three dominant eigenvalues are clearly separated from the rest. As a step further, only the three dominant eigenvalues are kept. The reconstructed signals are shown in Fig. 4.4b. It can be seen that the reconstructed signals are substantially smoother compared to those in Fig. 4.4a.

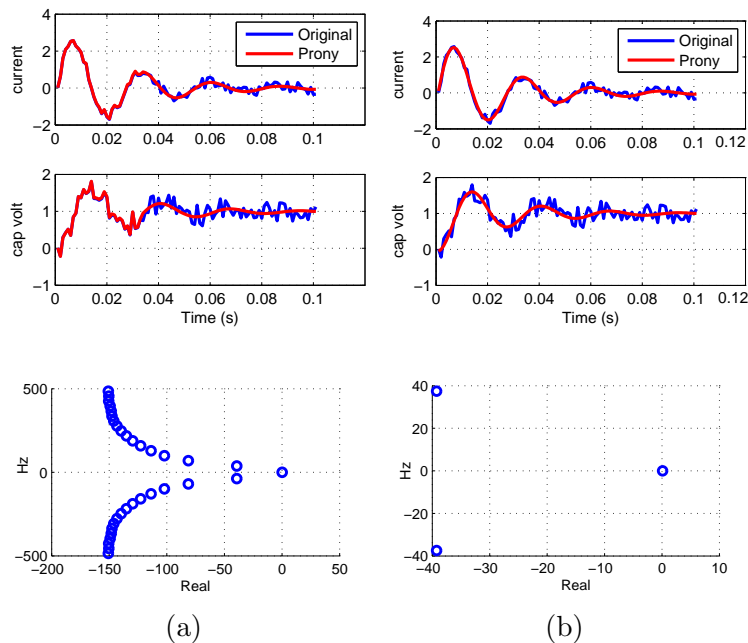


Figure 4.4: Reduced-order Prony analysis results of the RLC circuit. (4.4a) with Hankel matrix rank reduction. (4.4b) with rank reduction and eigenvalue reduction techniques.

A reduced-order Prony analysis has been developed using Hankel matrix rank reduction and eigenvalue reduction techniques. The improved Prony analysis shows that it can correctly identify the system poles from noisy signals.

4.4 Case Studies

Two more case studies are presented in this section which are large-scale power grid oscillations and real-world oscillation events. All of the proposed methods and simulations are implemented in MATLAB. The measurement data for the 16-machine 68-bus system are generated using the power system toolbox (PST) [48], which is a MATLAB-based power system dynamic simulation. The measurement data for the real-world oscillation events are generated using MATLAB.

4.4.1 Large-Scale Power Grid Oscillations

A large-scale power grid oscillations case study is presented in this section. The 16-machine 68-bus test case system (shown in Fig. 3.6) is used for eigenvalue estimation of large-scale power grid oscillations. As discussed in Chapter 3 (Section 3.4.2), this system represents the New England Test System (NETS)-New York Power System (NYPS) interconnected system [52] and has five areas. NETS is represented by area 4 which has generators G1 to G9, while NYPS is represented by area 5 which has generators G10 to G13. Three other areas have equivalent generators G14 to G16.

Simulation results are produced by power system toolbox (PST) [48]. The dynamic event applied is a three-phase fault on line 29-28 at Bus 28 side. It is cleared in 0.01 seconds and the line is tripped after another 0.05 seconds. Dynamic simulation data after the line tripping are used for eigenvalue estimation.

The network assumes algebraic voltage and current relationship, while the 16 machines are modeled as second-order system. Small signal analysis of PST gives 32 eigenvalues. Among them, four pairs of complex conjugate eigenvalues correspond to inter-area oscillation modes with frequency in the range of 0.3 Hz to 0.8 Hz.

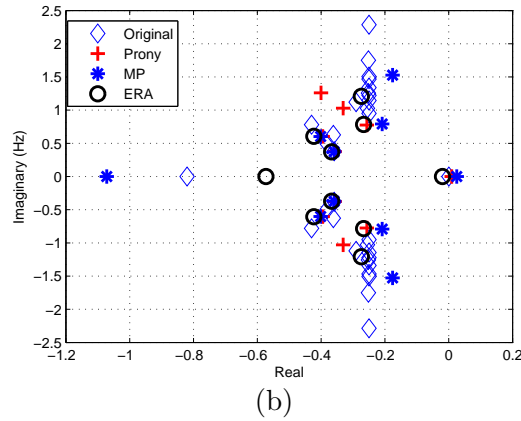
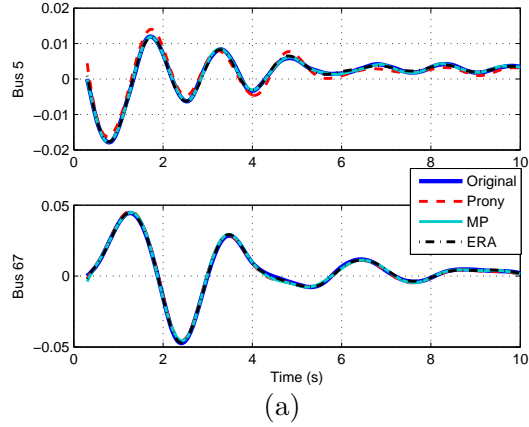


Figure 4.5: Large-scale power grid oscillation signal reconstruction and eigenvalue estimation (Order is 10).

In this case study, eigenvalues from a reduced-order system are sought based on measurements. First, the system is assumed to have an order of 10 as this five-area system is known to be represented by five equivalent generators, each of two orders [74].

Two voltage deviation signals in different areas (Bus 5 in Area 4 and Bus 67 in Area 1) are chosen for eigenvalue estimation and signal reconstruction. Those two signals are re-sampled with sampling time interval of 0.02 s. Further, Bus 67's signal is scaled up 100 times to be in the same order as that from Bus 5. The time periods for all tests are 10 seconds.

Original Prony analysis without rank reduction cannot give adequate reconstructed signals even with high orders. Therefore, the proposed reduced-order Prony analysis is applied. The number of samples is $N = 486$ for each measurement data. The Hankel matrix width for the rank reduced Prony analysis is set to be 250. The L parameter for MP and ERA is chosen as 180. Reduced-order Prony analysis can provide accurate reconstructed signals as MP and ERA, shown in Fig. 4.5a. The estimated eigenvalues of the three methods are shown in Fig. 4.5b. It can be seen that all three methods give accurate signal matching results. In addition, seven eigenvalues, including one at the origin, three modes at 0.37 Hz , 0.6 Hz, and 0.78 Hz, are identified by all three methods.

Further order reduction is applied to test the capability of each method. The number of the order is reduced to be 4. Fig. 4.6 presents the estimation results when the order is assumed as 4. It can be seen that ERA and reduced-order Prony lead to good signal matching results. Two inter-area oscillation modes are identified by these two methods. On the other hand, MP does not give good signal matching results. MP identifies one mode in the inter-area oscillation frequency range, and two real eigenvalues with one at the origin and another further left.

The three methods can all give reduced-order eigenvalues for power grid oscillation case study. Reduced-order Prony and ERA show stronger capability in handling reduced-order systems compared to MP.

4.4.2 Real-World Oscillation Events

In order to validate the effectiveness of the proposed methods, real-world oscillation events are analyzed. A test cases library of power system oscillations is presented in [75], and the real-world oscillation data can be found in [76]. The oscillation events are captured by Independent System Operator-New England (ISO-NE), which is a part of the eastern interconnection in the United States. PMU measurements are collected from different locations

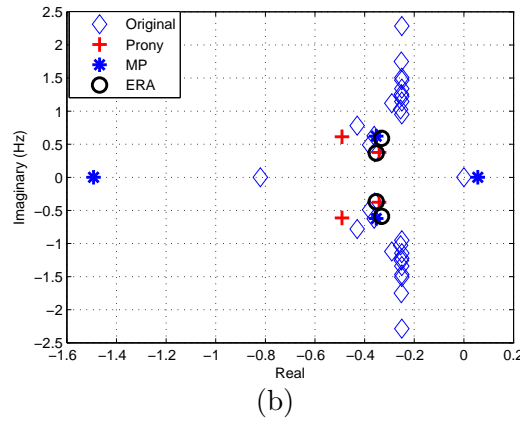
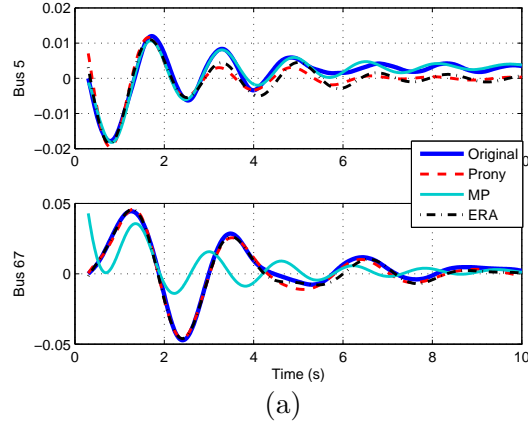


Figure 4.6: Large-scale power grid oscillation signal reconstruction and eigenvalue estimation (Order is 4).

of the ISO-NE system during the oscillatory events. Two oscillation events are investigated and analyzed in this section. The simulation results are carried out in MATLAB.

4.4.2.1 Oscillation Event 1

Oscillation Event 1 occurred on June 17, 2016 with a dominant mode of 0.27 Hz due to an issue of a generator in the southern area of the eastern interconnection which is out of the ISO-NE area [76]. The PMU measurements are provided for the first 3 minutes of this oscillation event. Phase-to-ground voltage magnitudes are shown in Fig. 4.7a. Two

voltage signals from different substations are selected: Signal 5 (Substation 2) and Signal 13 (Substation 5). The voltage measurements from 40 to 60 seconds are analyzed to detect the inter-area oscillation. The sampling rate is 0.034 seconds, and the number of samples is 601. The Hankel matrix width of the reduced-order Prony analysis is 280, while L parameter for ERA and MP is 200.

First, the system order is assumed as 15 to test the ability of the three methods to identify the inter-area oscillation. All of the three methods can provide accurate reconstructed signals compared to the original measurements as shown in Fig. 4.8a. The estimated eigenvalues are presented in Fig. 4.8b. It can be seen that the three methods can identify the oscillation mode of 0.27 Hz. The proposed Prony analysis has the dominant mode on the right half-plane (RHP), and the refined ERA has the dominant mode far right compared to the other modes. On the other hand, MP has three additional pair of complex conjugate eigenvalues on the RHP along with the dominant mode. This gives an advantage to the proposed Prony analysis and ERA which can clearly specify the dominant modes.

In addition, the system order is reduced to be 3 to investigate the effect of the order assumptions. Fig. 4.9 presents the reconstructed signals and the estimated eigenvalues of the three methods when the order is assumed as 3. It can be observed that the three methods have adequate reconstructed signals compared to the original signals. Also, all of the three methods can identify the dominant mode of 0.27 Hz.

4.4.2.2 Oscillation Event 2

Oscillation Event 2 occurred on October 3, 2017 due to an issue of a generator governor outside of the ISO-NE, and it has three dominant modes of 0.08, 0.15, and 0.31 Hz [76]. Six minutes of this oscillatory event are provided from PMU data. Those PMU measurements contain some bad data which should be removed to get the correct signals. Fig. 4.7b presents the phase-to-ground voltage magnitudes of this event. To identify the inter-area

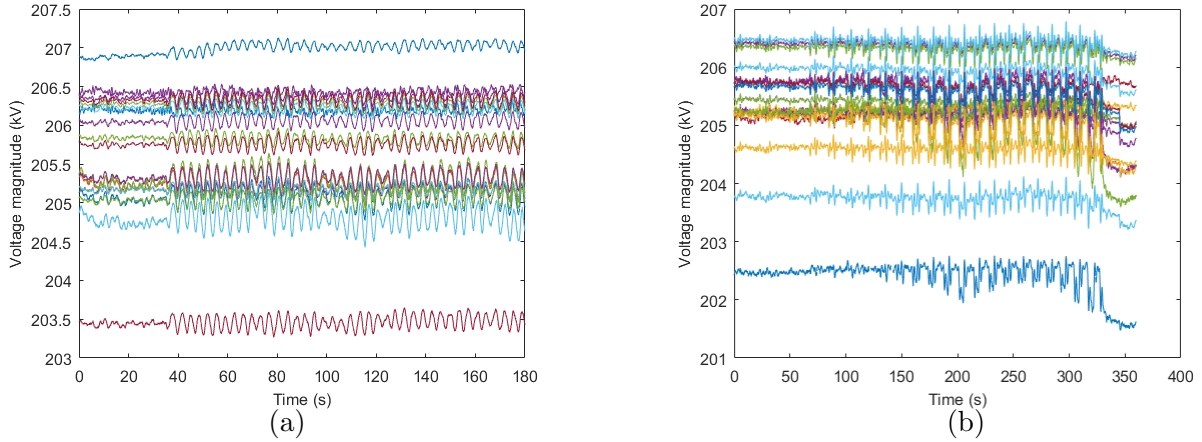


Figure 4.7: Phase-to-ground voltage magnitudes during the oscillatory events. (4.7a) Event 1. (4.7b) Event 2.

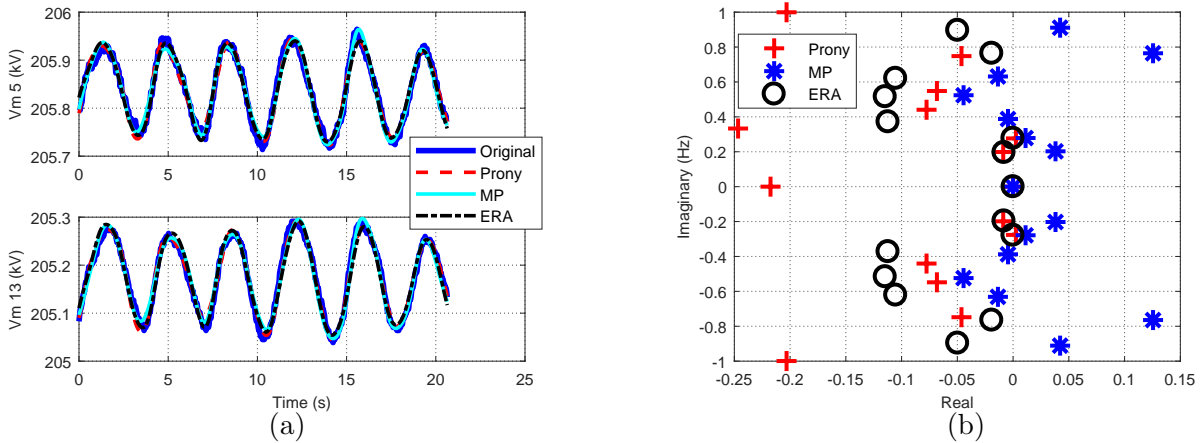


Figure 4.8: Signal reconstruction and eigenvalue estimation of Event 1 with assumed order of 15.

modes, the voltage measurements from 270 to 300 seconds are analyzed, and all of the signals are considered in this case. The number of samples is 901, and the sampling rate is 0.034 seconds. The Hankel matrix width of the three methods is 400.

To examine the capability of each method, the system order is assumed as 15. All of the three methods have accurate reconstructed signals as shown in Fig. 4.10a. The estimated eigenvalues of this case are shown in Fig. 4.10b. It can be seen that the proposed Prony analysis and ERA clearly have the three dominant modes on the RHP. In contrast, MP has

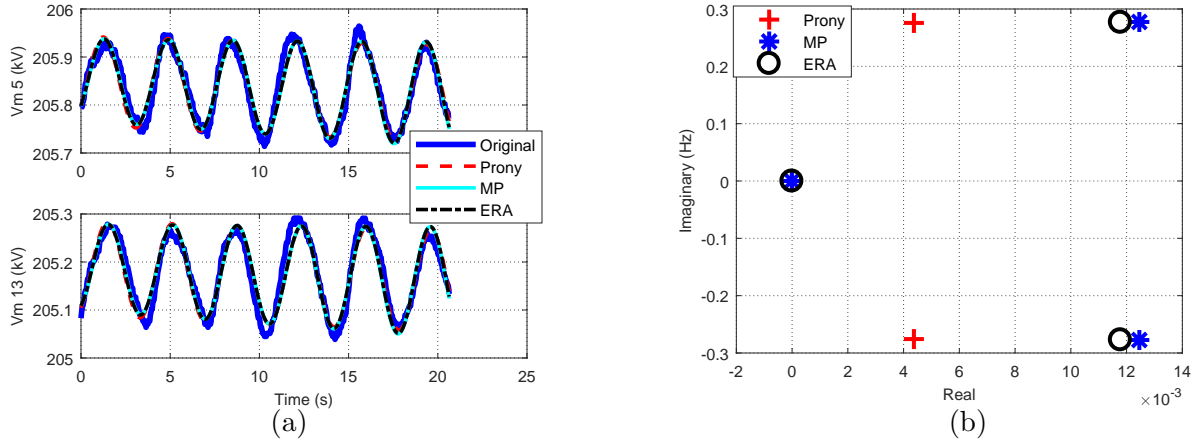


Figure 4.9: Signal reconstruction and eigenvalue estimation of Event 1 with assumed order of 3.

two dominant modes (0.15 and 0.31 Hz) on the RHP and one mode of 0.08 Hz on the LHP which can be difficult to specify the dominant modes for this method. It should be noted that the three methods have one additional pair of complex conjugate eigenvalues on the RHP. Lower orders such as 3 or 4 cannot provide accurate reconstructed signals and may not detect some of the inter-area oscillations of Event 2. Note that order 15 is the lowest order that can obtain well-matched reconstructed signals in this case.

The dominant modes of the real-world oscillation events can be identified with accuracy for the three methods. Reduced-order Prony analysis and ERA can easily specify the dominant modes from the other modes.

4.4.3 Development Discussion

The three measurement-based identification methods are investigated in this chapter. Prony analysis method is improved to achieve reduced-order system eigenvalue identification and noise resilience. Traditional Prony analysis cannot obtain adequate reconstructed signals and detect the inter-area oscillations with low order assumptions especially in the case of noisy signals as discussed in Section 4.3. In addition, traditional ERA Hankel matrices

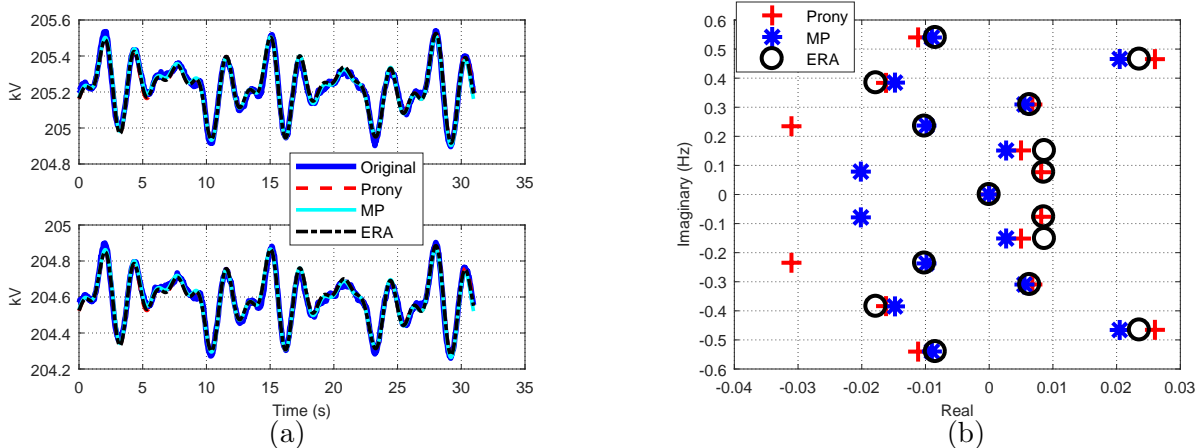


Figure 4.10: Event 2 signal reconstruction and eigenvalue estimation.

are improved to handle multi-channel data, and the rank reduction technique is applied to the second shifted Hankel matrix of ERA to enhance its performance. Hence, the reduced-order Prony analysis and refined ERA have a better performance in detecting the inter-area oscillation modes and providing the reconstructed signals compared to the traditional approaches.

Different order assumptions are tested and investigated in this chapter. The chosen order should be low to adequately identify the dominant modes. The best order assumption is the lowest order that can provide accurate reconstructed signals. This lowest order can clearly detect the inter-area oscillation modes. Order assumptions from 3 to 20 are most effective orders with different systems and PMU measurements, and the lowest one which can provide well-matched signals should be chosen.

The computational time of the three methods is compared as shown in Table 4.1. The three methods have similar CPU time when the number of samples is not large, while MP has a better CPU time compared to reduced-order Prony analysis and ERA in the case of the large number of samples. Although MP is faster in this case, the proposed Prony analysis and ERA have a superior result. It can also be seen that the reduced-order Prony analysis and MP are faster compared to ERA when the number of analyzed signals is large.

Table 4.1: CPU time comparison of the three methods

System	Number of Samples	Number of Signals	Simulation Time (s)	CPU Time (s)		
				Prony	ERA	MP
NETS-NYPS	486	2	10	0.4531	0.4688	0.4063
ISO-NE (Event 1)	601	2	20	0.5625	0.5625	0.4375
ISO-NE (Event 2)	901	25	30	18.7188	47.2031	18.2969

Prony analysis, MP, and ERA have proven their capabilities with low orders to identify the inter-area oscillations in different power system applications including real-world oscillatory events.

4.5 Conclusion

This chapter examines the principles, multi-channel data handling, and noise resilience techniques of three eigenvalue identification methods used in power systems: Prony analysis, Matrix Pencil (MP), and Eigensystem Realization Algorithm (ERA). SVD-based rank reduction technique is identified as the key to noise resilience and order reduction. Accordingly, ERA method is refined by applying SVD-based rank reduction on both Hankel matrices. A reduced-order Prony analysis method through Hankel matrix rank reduction is invented. The new Prony analysis can accurately identify system eigenvalues from noisy signals. Three case studies are presented to illustrate the three methods, including a tutorial example on RLC circuit resonance, a large-scale power grid oscillation example, and real-world oscillation events. The case study results demonstrate the efficacy of all three methods in accurate eigenvalue identification.

Chapter 5: Conclusion and Future Work

5.1 Conclusion

Phasor measurement units (PMUs) are investigated in this research including three main objectives. First, optimal PMU placement (OPP) problem to reduce the number of PMUs required to make the system fully observable is discussed. MILP zero injection formulation is improved to overcome the observability redundancy and optimality drawbacks. A new formulation for nonlinear programming-based PMU placement for zero injection measurement is proposed and validated to provide the least number of PMUs compared to other methods. Second, singular values of the Hankel matrix are demonstrated for Prony analysis to serve as an indicator for estimation accuracy. Signals with large observability also show large singular values. The influence of model order and noise level is also demonstrated by the singular values. Third, three eigenvalue identification methods used in power systems, which are Prony analysis, Matrix Pencil (MP), and Eigensystem Realization Algorithm (ERA), are examined. The principles, multi-channel data handling, and noise resilience techniques of three approached are presented. SVD-based rank reduction technique is identified as the key to noise resilience and order reduction. ERA method is refined by applying SVD-based rank reduction on both Hankel matrices, and a reduced-order Prony analysis method is invented through Hankel matrix rank reduction. The new Prony analysis can accurately identify system eigenvalues from noisy signals.

5.2 Future Work

A dynamic parameter estimation technique using the measurement-based methods can be investigated in the future. Using the PMU data and measurement-based methods of the system identification can give an accurate dynamic parameter estimation without prior information of the system transfer function. Generator parameters such as inertia constant, damping coefficients, and regulation speed constant can be estimated. The following sections discuss the background and present the initial results of the dynamic parameter estimation using the proposed reduced-order Prony analysis.

5.2.1 Dynamic Parameter Estimation Background

Simulation accuracy can improve the safety and efficiency of the operation of power systems by providing the security margins and transfer limits [77]. Using PMU data and measurement-based methods of the system identification can give dynamic parameter estimation. In practical, the dynamic parameters provided by the manufacturer can be inaccurate due to several reasons such as aging, repairs, or unrecorded gain settings [78]. These inaccurate parameters can cause a deviation in the simulated and actual dynamic response. Therefore, power utilities rely on the dynamic parameter estimation to provide accurate estimation of the generators and enhance the security of power systems.

Dynamic parameter estimation has been investigated in the literature. Based on data, time-domain data based are examined in [79–86], while the frequency response data based are discussed in [87–89]. Based on measurements, parameter estimation is obtained with methods as digital fault recorder and high sampling interval [83, 85], excitation with step sequence inputs [80, 82], short circuit test methods [79, 84], and offline test approaches [87–89]. Based on the parameter type, both electrical and mechanical parameters are estimated in [80, 82, 86], and only electrical parameter estimation is provided in [79, 83–85, 87–89].

In addition, dynamic parameter estimation can be classified into two categories based on the mathematical estimation approach which are least square estimation and Kalman filter estimation. Parameter estimation is formulated as least squares estimation (LSE) in [79–82,84,87,89]. Kalman filter is used to estimate the dynamic parameters in [86,90–92]. LSE-based dynamic parameter identification using discrete autoregression exogenous (ARX) model is presented in [93]. However, many of these techniques assume high order model or known model structure, e.g., [81,82,86].

PMU data based estimation is considered as online and time-domain estimation which has the capability of estimating the electrical and mechanical related parameters. The majority of the research in the literature is related to the LSE parameter estimation based on the time-domain or frequency response data. A few research can be found on LSE dynamic parameter estimation based on PMU data identification. PMU data based estimation is limited to state estimation [94] or dynamic state estimation for the second-order mechanical system [91,95–97]. However, those approaches are based on Kalman filter estimation that requires to have a prior information of the transfer function of the power system to formulate the Kalman estimator which may not be available in real applications.

This future work presents a new dynamic parameter estimation technique using rank-reduced Prony analysis methods. A rank-reduced Prony analysis to identify the system eigenvalues with reduced order has been discussed in Chapter 4. The proposed approach is LSE-based dynamic parameter estimation using PMU data. The model structure is assumed to be unknown, and a reduced-order model is achieved. This proposed technique is solved with two main stages. At Stage 1, the eigenvalues are obtained using rank-reduced Prony analysis which can accurately identify the eigenvalues with reduced-order model. At Stage 2, the A matrix and the system parameters are found by solving a nonlinear optimization problem. The nonlinear optimization problem is solved by MATLAB toolbox YALMIP [98] with IPOPT solver [99].

5.2.2 Two-Machine Power System Model

The two-machine power system model (shown in Fig. 5.1) and the simplified turbine model (shown in Fig. 5.2) are used as a reduced system for the dynamic parameter estimation. The positions of the rotor's q-axis of the two machines are represented by δ_1 and δ_2 . If we assume that the speed (ω) in per unit, we can get the following [100]:



Figure 5.1: Two-machine power system model.

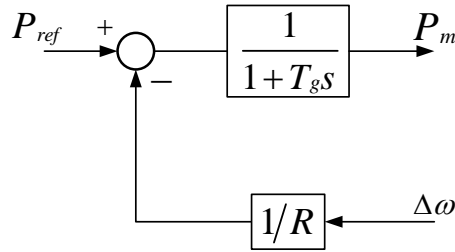


Figure 5.2: Turbine model block diagram.

$$\dot{\delta}_1 = \omega_0(\omega_1 - 1) \quad (5.1)$$

where $\Delta\omega = \omega_1 - \omega_0$, and ω_0 is a constant nominal speed. Then (5.1) can be linearized at an equilibrium point as follows.

$$\Delta\dot{\delta}_1 = \omega_0\Delta\omega_1 \quad (5.2)$$

Note that the linearization is evaluated at x_0 as the following:

$$\Delta f = \left. \frac{\partial f}{\partial x} \right|_{x_0} \Delta x \quad (5.3)$$

The swing equation in per unit can be represented as follows [100].

$$\dot{\omega}_1 = \frac{1}{2H_1}(P_{m1} - P_{e1} - D_1\Delta\omega_1) \quad (5.4)$$

where H_1 is kinetic energy ratio of the rotor and the power base at a constant nominal speed, P_{m1} is the mechanical power, P_{e1} is the electrical power, and D_1 is the damping coefficient.

After that, the swing equation (5.4) is linearized at initial conditions to result in the following [100]:

$$\Delta\dot{\omega}_1 = \frac{1}{2H_1}(\Delta P_{m1} - \Delta P_{e1} - D_1\Delta\omega_1) \quad (5.5)$$

From the linearized model, the electrical power can be obtained as follows.

$$P_{e1} = -P_{e2} = \frac{E_1 E_2}{X} \sin \delta_{12} \quad (5.6)$$

$$\Delta P_{e1} = -\Delta P_{e2} = \frac{E_1 E_2}{X} \cos \delta_{12} (\Delta\delta_1 - \Delta\delta_2) \quad (5.7)$$

Then (5.5) can be expressed as follows.

$$\Delta\dot{\omega}_1 = \frac{1}{2H_1}(\Delta P_{m1} - T(\Delta\delta_1 - \Delta\delta_2) - D_1\Delta\omega_1) \quad (5.8)$$

where T is given by the following:

$$T = \frac{E_1 E_2}{X} \cos \delta_{12} \quad (5.9)$$

From the turbine model as shown in Fig. 5.2, the mechanical power for Generator 1 can be found as:

$$P_{ref} - \frac{1}{R}\Delta\omega = P_m + T_g \frac{dP_m}{dt} \quad (5.10)$$

$$\dot{P}_{m1} = \frac{1}{T_{g1}}(P_{1,ref} - \frac{1}{R_1}\Delta\omega_1 - P_{m1}) \quad (5.11)$$

Equation (5.11) can be linearized at an equilibrium point as follows.

$$\Delta\dot{P}_{m1} = \frac{1}{T_{g1}}(-\frac{1}{R_1}\Delta\omega_1 - \Delta P_{m1}) \quad (5.12)$$

Thus, swing equations for Generator 1 are obtained. Similarly, the equations for Generator 2 can be provided. For simplification, δ_2 can be treated as the reference angle, or $\delta_1 - \delta_2$ can be used as state variables to get the following:

$$\begin{cases} \Delta\dot{\delta}_{12} = \omega_0(\Delta\omega_1 - \Delta\omega_2) \\ \Delta\dot{\omega}_1 = \frac{1}{2H_1}(\Delta P_{m1} - T\Delta\delta_{12} - D_1\Delta\omega_1) \\ \Delta\dot{P}_{m1} = \frac{1}{T_{g1}}(-\frac{1}{R_1}\Delta\omega_1 - \Delta P_{m1}) \\ \Delta\dot{\omega}_2 = \frac{1}{2H_2}(\Delta P_{m2} + T\Delta\delta_{12} - D_2\Delta\omega_2) \\ \Delta\dot{P}_{m2} = \frac{1}{T_{g2}}(-\frac{1}{R_2}\Delta\omega_2 - \Delta P_{m2}) \end{cases} \quad (5.13)$$

Therefore, the A matrix can be obtained as follows.

$$\dot{x} = \underbrace{\begin{bmatrix} 0 & \omega_0 & 0 & -\omega_0 & 0 \\ -\frac{T}{2H_1} & -\frac{D_1}{2H_1} & \frac{1}{2H_1} & 0 & 0 \\ 0 & -\frac{1}{T_{g1}R_1} & -\frac{1}{T_{g1}} & 0 & 0 \\ \frac{T}{2H_2} & 0 & 0 & -\frac{D_2}{2H_2} & \frac{1}{2H_2} \\ 0 & 0 & 0 & -\frac{1}{T_{g2}R_2} & -\frac{1}{T_{g2}} \end{bmatrix}}_A \underbrace{\begin{bmatrix} \Delta\delta_{12} \\ \Delta\omega_1 \\ \Delta P_{m1} \\ \Delta\omega_2 \\ \Delta P_{m2} \end{bmatrix}}_x \quad (5.14)$$

5.2.3 Formulation of the Dynamic Parameter Estimation

The proposed optimization problem can estimate the model structure and parameter from the eigenvalues that obtained from rank-reduced Prony analysis method (as discussed in Chapter 4). The model has nine parameters which are H_1 , H_2 , T , D_1 , D_2 , T_{g1} , T_{g2} , R_1 , and R_2 . Thus, the optimization problem will be as the following:

$$\min \sum_{i=1}^n e_i^2 \quad (5.15a)$$

$$\text{s.t.: } \det(\lambda_i I - A) + e_i = 0, \quad i = 1, 2, \dots, n. \quad (5.15b)$$

$$H_1 \geq 0, H_2 \geq 0, T \geq 0, D_1 \geq 0, \quad (5.15c)$$

$$D_2 \geq 0, T_{g1} \geq 0, T_{g2} \geq 0, \quad (5.15d)$$

$$R_1 \geq 0, R_2 \geq 0. \quad (5.15e)$$

where n is the number of the system order. If four parameters are fixed to be true values, the other five parameters can be found. On the other hand, if all parameters are unknown, the solution can also be found with prior information of multiple parameters range.

This is a nonlinear optimization problem which is solved by MATLAB toolbox YALMIP [98] with an IPOPT solver [99]. The unknown parameters of the A matrix are preferred to be on the numerator to avoid zero initial conditions, then the estimated values of H , T_g , and R parameters will be inverted. Therefore, the A matrix is re-written as follows.

$$\left[\begin{array}{ccc|cc} 0 & \omega_0 & 0 & -\omega_0 & 0 \\ -\frac{TH'_1}{2} & -\frac{D_1H'_1}{2} & \frac{H'_1}{2} & 0 & 0 \\ 0 & -T'_{g1}R'_1 & -T'_{g1} & 0 & 0 \\ \hline \frac{TH'_2}{2} & 0 & 0 & -\frac{D_2H'_2}{2} & \frac{H'_2}{2} \\ 0 & 0 & 0 & -T'_{g2}R'_2 & -T'_{g2} \end{array} \right] \quad (5.16)$$

5.2.4 Example

The simplified two-machine power system is modeled using power system toolbox (PST) [48]. Rank-reduced Prony analysis as explained in Chapter 4 is applied for eigenvalue estimation. The system order is assumed to be 5 with two pairs of complex conjugate eigenvalues and a real one. The estimated eigenvalues are $\lambda = [-0.31111 \pm 10.359i, -0.13364 \pm 5.1774i, -5.7129 \times 10^{-5}]^T$.

Then the constraints for the nine parameters are added with the prior information of the system. The feasible region can be reduced with adding an acceptable range for some parameters. Also, it is assumed that $H'_1 = H'_2$ and $D_1 = D_2$ since the two systems have the same size and damping coefficient. Thus, eleven constraints are added to the optimization problem as follows.

$$\begin{aligned} \min \quad & \sum_{i=1}^5 e_i^2 \\ \text{s.t.:} \quad & \det(\lambda_i I - A) + e_i = 0, \quad i = 1, 2, \dots, 5. \\ & H'_1 \geq 0, \quad H'_2 \geq 0, \\ & 20 \geq T \geq 1.6, \\ & 100 \geq D_1 \geq 1, \quad 100 \geq D_2 \geq 1, \\ & T'_{g1} \geq 0, \quad T'_{g2} \geq 0, \\ & 100 \geq R'_1 \geq 1, \quad 100 \geq R'_2 \geq 1, \\ & H'_1 = H'_2, \quad D_1 = D_2. \end{aligned}$$

The above nonlinear optimization problem is solved using MATLAB toolbox YALMIP [98] with IPOPT solver [99]. The actual values and estimated values of the two-machine power system model parameters are shown in Table 5.1. The number of the iteration in this optimization problem is 196, while the overall nonlinear problem error is 1.18×10^{-9} .

Table 5.1: Two-machine model parameter estimation result

Parameter	Actual Value	Estimated Value
H_1	6.5	6.5569
D_1	6	3.5271
T_{g1}	0.5	0.49294
R_1	0.04	0.01
H_2	6.5	6.5569
D_2	6	3.5271
T_{g2}	0.5	0.49294
R_2	0.04	0.01
T	2	1.6

5.2.4.1 Sensitivity Analysis

Parameter estimation can be improved by having some of the parameters fixed or reducing the feasible range with prior information of the system. For example, if the lower bound of parameter T is set to be 2 ($20 \geq T \geq 2$), this can result in a better estimation. In this case, the reduced feasible regions of D_1 and D_2 are not required (i.e., $D_1 \geq 0$ and $D_2 \geq 0$). Therefore, only three feasible regions of T , R'_1 , and R'_2 are reduced by an acceptable range with prior information of the system. Table 5.2 shows the results of the parameter estimation with 2 as a lower bound of T feasible region. The number of iterations and the overall nonlinear problem error are 276 and 5.91×10^{-12} , respectively. In addition, the estimation result can also be more accurate when the lower bounds of parameters D_1 and D_2 are set to be 6 ($100 \geq D_1 \geq 6$ and $100 \geq D_2 \geq 6$) as can be seen from Table 5.3. With those two constraints, the constraint $D_1 = D_2$ will be no longer needed. Therefore, the number of constraints is reduced to 10 instead of 11. The resulted number of iterations in this case is 107, whereas the nonlinear problem error is 1.24×10^{-8} .

Table 5.2: Parameter estimation with different lower bound of T

Parameter	Actual Value	Estimated Value
H_1	6.5	7.9835
D_1	6	5.1725
T_{g1}	0.5	0.48802
R_1	0.04	0.01
H_2	6.5	7.9835
D_2	6	5.1725
T_{g2}	0.5	0.48802
R_2	0.04	0.01
T	2	2.00

Table 5.3: Parameter estimation with different lower bounds of D_1 and D_2

Parameter	Actual Value	Estimated Value
H_1	6.5	6.4665
D_1	6	6.00
T_{g1}	0.5	0.55315
R_1	0.04	0.01
H_2	6.5	6.4665
D_2	6	6.00
T_{g2}	0.5	0.55315
R_2	0.04	0.01
T	2	1.6

References

- [1] A. G. Phadke, "Synchronized phasor measurements in power systems," *IEEE Computer Applications in power*, vol. 6, no. 2, pp. 10–15, 1993.
- [2] B. Xu and A. Abur, "Observability analysis and measurement placement for systems with PMUs," in *IEEE Power Systems Conference and Exposition*, 2004, pp. 943–946.
- [3] M. Hurtgen and J. C. Maun, "Advantages of power system state estimation using phasor measurement units," in *16th Power Systems Computation Conference*, 2008, pp. 1–7.
- [4] North American SynchroPhasor Initiative (NASPI). [Online]. Available: <https://www.naspi.org/node/372>; <https://www.naspi.org/node/407>
- [5] R. F. Nuqui, "State estimation and voltage security monitoring using synchronized phasor measurements," Ph.D. dissertation, Virginia Tech, 2001.
- [6] M. Young and A. Silverstein, "Factors affecting pmu installation costs," *U.S. Department of Energy - Office of Electricity Delivery and Energy Reliability*, 2014. [Online]. Available: <https://www.energy.gov/sites/prod/files/2014/11/f19/SG-PMU-cost-study-Oct2014.pdf>
- [7] B. Gou, "Generalized integer linear programming formulation for optimal PMU placement," *IEEE Transactions on Power Systems*, vol. 23, no. 3, pp. 1099–1104, 2008.
- [8] M. Crow, M. Gibbard, A. Messina, J. Pierre, J. Sanchez-Gasca, D. Trudnowski, and D. Vowles, "Identification of electromechanical modes in power systems," *IEEE Task Force Report, Special Publication TP462*, 2012.
- [9] J. Sanchez-Gasca and J. Chow, "Computation of power system low-order models from time domain simulations using a hankel matrix," *IEEE Transactions on Power Systems*, vol. 12, no. 4, pp. 1461–1467, 1997.
- [10] A. Almunif and L. Fan, "Optimal pmu placement for modeling power grid observability with mathematical programming methods," *International Transactions on Electrical Energy Systems*, p. e12182, 2019.

- [11] T. Baldwin, L. Mili, M. Boisen, and R. Adapa, "Power system observability with minimal phasor measurement placement," *IEEE Transactions on Power Systems*, vol. 8, no. 2, pp. 707–715, 1993.
- [12] K.-S. Cho, J.-R. Shin, and S. H. Hyun, "Optimal placement of phasor measurement units with gps receiver," in *Power Engineering Society Winter Meeting, 2001. IEEE*, vol. 1. IEEE, 2001, pp. 258–262.
- [13] G. Denegri, M. Invernizzi, and F. Milano, "A security oriented approach to pmu positioning for advanced monitoring of a transmission grid," in *Power System Technology, 2002. Proceedings. PowerCon 2002. International Conference on*, vol. 2. IEEE, 2002, pp. 798–803.
- [14] F. Marin, F. Garcia-Lagos, G. Joya, and F. Sandoval, "Genetic algorithms for optimal placement of phasor measurement units in electric networks," *Electron. Lett.*, vol. 39, no. 19, pp. 1403–1405, 2003.
- [15] B. Milosevic and M. Begovic, "Nondominated sorting genetic algorithm for optimal phasor measurement placement," *IEEE Transactions on Power Systems*, vol. 18, no. 1, pp. 69–75, 2003.
- [16] J. Peng, Y. Sun, and H. Wang, "Optimal pmu placement for full network observability using tabu search algorithm," *International Journal of Electrical Power & Energy Systems*, vol. 28, no. 4, pp. 223–231, 2006.
- [17] M. Hajian, A. Ranjbar, T. Amraee, and A. Shirani, "Optimal placement of phasor measurement units: Particle swarm optimization approach," in *Intelligent Systems Applications to Power Systems, 2007. ISAP 2007. International Conference on*. IEEE, 2007, pp. 1–6.
- [18] N. C. Koutsoukis, N. M. Manousakis, P. S. Georgilakis, and G. N. Korres, "Numerical observability method for optimal phasor measurement units placement using recursive tabu search method," *IET Generation, Transmission & Distribution*, vol. 7, no. 4, pp. 347–356, 2013.
- [19] F. Aminifar, C. Lucas, A. Khodaei, and M. Fotuhi-Firuzabad, "Optimal placement of phasor measurement units using immunity genetic algorithm," *IEEE Transactions on power delivery*, vol. 24, no. 3, pp. 1014–1020, 2009.
- [20] S. Chakrabarti, G. K. Venayagamoorthy, and E. Kyriakides, "Pmu placement for power system observability using binary particle swarm optimization," in *Power Engineering Conference, 2008. AUPEC'08. Australasian Universities*. IEEE, 2008, pp. 1–5.
- [21] A. Ahmadi, Y. Alinejad-Beromi, and M. Moradi, "Optimal pmu placement for power system observability using binary particle swarm optimization and considering measurement redundancy," *Expert Systems with Applications*, vol. 38, no. 6, pp. 7263–7269, 2011.

- [22] D. Dua, S. Dambhare, R. K. Gajbhiye, and S. Soman, "Optimal multistage scheduling of PMU placement: An ILP approach," *IEEE Transactions on Power Delivery*, vol. 23, no. 4, pp. 1812–1820, 2008.
- [23] N. H. Abbasy and H. M. Ismail, "A unified approach for the optimal PMU location for power system state estimation," *IEEE Transactions on Power Systems*, vol. 24, no. 2, pp. 806–813, 2009.
- [24] B. Xu and A. Abur, "Optimal placement of phasor measurement units for state estimation," in *Power Systems Engineering Research Center, PSERC*, 2005.
- [25] M. Korkali and A. Abur, "Placement of pmus with channel limits," in *Power & Energy Society General Meeting, 2009. PES'09. IEEE*. IEEE, 2009, pp. 1–4.
- [26] —, "Impact of network sparsity on strategic placement of phasor measurement units with fixed channel capacity," in *Circuits and Systems (ISCAS), Proceedings of 2010 IEEE International Symposium on*. IEEE, 2010, pp. 3445–3448.
- [27] S. M. Mahaei and M. T. Hagh, "Minimizing the number of pmus and their optimal placement in power systems," *Electric Power Systems Research*, vol. 83, no. 1, pp. 66–72, 2012.
- [28] E. Abiri, F. Rashidi, and T. Niknam, "An optimal pmu placement method for power system observability under various contingencies," *International Transactions on Electrical Energy Systems*, vol. 25, no. 4, pp. 589–606, 2015.
- [29] F. Aminifar, A. Khodaei, M. Fotuhi-Firuzabad, and M. Shahidehpour, "Contingency-constrained pmu placement in power networks," *IEEE Transactions on Power Systems*, vol. 25, no. 1, pp. 516–523, 2010.
- [30] M. Esmaili, K. Gharani, and H. A. Shayanfar, "Redundant observability pmu placement in the presence of flow measurements considering contingencies," *IEEE Transactions on Power Systems*, vol. 28, no. 4, pp. 3765–3773, 2013.
- [31] K. G. Khajeh, E. Bashar, A. M. Rad, and G. B. Gharehpetian, "Integrated model considering effects of zero injection buses and conventional measurements on optimal pmu placement," *IEEE Transactions on Smart Grid*, vol. 8, no. 2, pp. 1006–1013, 2017.
- [32] S. Chakrabarti, E. Kyriakides, and D. G. Eliades, "Placement of synchronized measurements for power system observability," *IEEE Transactions on Power Delivery*, vol. 24, no. 1, pp. 12–19, 2009.
- [33] N. M. Manousakis and G. N. Korres, "A weighted least squares algorithm for optimal PMU placement," *IEEE Transactions on Power Systems*, vol. 28, no. 3, pp. 3499–3500, 2013.

- [34] N. Theodorakatos, N. Manousakis, and G. Korres, “Optimal PMU placement using nonlinear programming,” *OPT -i: An International Conference on Engineering and Applied Sciences Optimization*, pp. 240–258, 2015.
- [35] N. P. Theodorakatos, N. M. Manousakis, and G. N. Korres, “A sequential quadratic programming method for contingency-constrained phasor measurement unit placement,” *International Transactions on Electrical Energy Systems*, vol. 25, no. 12, pp. 3185–3211, 2015.
- [36] —, “Optimal placement of phasor measurement units with linear and non-linear models,” *Electric Power Components and Systems*, vol. 43, no. 4, pp. 357–373, 2015.
- [37] A. Almunif and L. Fan, “Mixed integer linear programming and nonlinear programming for optimal pmu placement,” in *2017 North American Power Symposium (NAPS)*. IEEE, 2017, pp. 1–6.
- [38] Power systems test case archive. [Online]. Available: <https://www2.ee.washington.edu/research/pstca/>
- [39] R. F. Nuqui and A. G. Phadke, “Phasor measurement unit placement techniques for complete and incomplete observability,” *IEEE Transactions on Power Delivery*, vol. 20, no. 4, pp. 2381–2388, 2005.
- [40] R. D. Zimmerman, C. E. Murillo-Sánchez, and R. J. Thomas, “Matpower: Steady-state operations, planning, and analysis tools for power systems research and education,” *IEEE Transactions on power systems*, vol. 26, no. 1, pp. 12–19, 2010.
- [41] A. Almunif and L. Fan, “Pmu measurements for oscillation monitoring: Connecting prony analysis with observability,” accepted, in *Power and Energy Society General Meeting (PES), 2019 IEEE*. IEEE, 2019, pp. 1–5.
- [42] J. F. Hauer, C. Demeure, and L. Scharf, “Initial results in prony analysis of power system response signals,” *IEEE Transactions on power systems*, vol. 5, no. 1, pp. 80–89, 1990.
- [43] D. Trudnowski, J. Johnson, and J. Hauer, “Making prony analysis more accurate using multiple signals,” *Power Systems, IEEE Transactions on*, vol. 14, no. 1, pp. 226–231, 1999.
- [44] L. Fan, “Data fusion-based distributed prony analysis,” *Electric Power Systems Research*, vol. 143, pp. 634–642, 2017.
- [45] N. Zhou, J. Pierre, and D. Trudnowski, “Some considerations in using prony analysis to estimate electromechanical modes,” in *Power and Energy Society General Meeting (PES), 2013 IEEE*. IEEE, 2013, pp. 1–5.

- [46] J.-H. Peng and N.-K. Nair, “Adaptive sampling scheme for monitoring oscillations using prony analysis,” *IET generation, transmission & distribution*, vol. 3, no. 12, pp. 1052–1060, 2009.
- [47] M. Dehghani, B. Shayanfard, and A. R. Khayatian, “Pmu ranking based on singular value decomposition of dynamic stability matrix,” *IEEE Transactions on Power Systems*, vol. 28, no. 3, pp. 2263–2270, 2013.
- [48] J. H. Chow and K. W. Cheung, “A toolbox for power system dynamics and control engineering education and research,” *IEEE transactions on Power Systems*, vol. 7, no. 4, pp. 1559–1564, 1992.
- [49] J. Khazaei, L. Fan, W. Jiang, and D. Manjure, “Distributed prony analysis for real-world pmu data,” *Electric Power Systems Research*, vol. 133, pp. 113–120, 2016.
- [50] J. H. Chow, A. Chakraborty, L. Vanfretti, and M. Arcaç, “Estimation of radial power system transfer path dynamic parameters using synchronized phasor data,” *IEEE Transactions on Power Systems*, vol. 23, no. 2, pp. 564–571, 2008.
- [51] P. W. Sauer, M. Pai, and J. H. Chow, *Power system dynamics and stability: with synchrophasor measurement and power system toolbox*. John Wiley & Sons, 2017.
- [52] G. Rogers, *Power system oscillations*. Springer Science & Business Media, 2012.
- [53] S. Brahma, R. Kavasseri, H. Cao, N. Chaudhuri, T. Alexopoulos, and Y. Cui, “Real-time identification of dynamic events in power systems using pmu data, and potential applications—models, promises, and challenges,” *IEEE Transactions on Power Delivery*, vol. 32, no. 1, pp. 294–301, 2017.
- [54] P. Kundur, N. J. Balu, and M. G. Lauby, *Power system stability and control*. McGraw-hill New York, 1994, vol. 7.
- [55] A. Almunif, L. Fan, and Z. Miao, “A tutorial on data-driven eigenvalue identification: Prony analysis, matrix pencil and eigensystem realization algorithm,” *submitted, International Transactions on Electrical Energy Systems*, 2019.
- [56] G. Liu, J. Ning, Z. Tashman, V. M. Venkatasubramanian, and P. Trachian, “Oscillation monitoring system using synchrophasors,” in *2012 IEEE Power and Energy Society General Meeting*. IEEE, 2012, pp. 1–8.
- [57] N. Zhou, J. W. Pierre, D. J. Trudnowski, and R. T. Guttromson, “Robust rls methods for online estimation of power system electromechanical modes,” *IEEE Transactions on Power Systems*, vol. 22, no. 3, pp. 1240–1249, 2007.
- [58] R. W. Wies, J. W. Pierre, and D. J. Trudnowski, “Use of arma block processing for estimating stationary low-frequency electromechanical modes of power systems,” *IEEE Transactions on Power Systems*, vol. 18, no. 1, pp. 167–173, 2003.

- [59] N. Zhou, D. J. Trudnowski, J. W. Pierre, and W. A. Mittelstadt, "Electromechanical mode online estimation using regularized robust rls methods," *IEEE Transactions on Power Systems*, vol. 23, no. 4, pp. 1670–1680, 2008.
- [60] J. W. Pierre, D. J. Trudnowski, and M. K. Donnelly, "Initial results in electromechanical mode identification from ambient data," *IEEE Transactions on Power Systems*, vol. 12, no. 3, pp. 1245–1251, 1997.
- [61] D. J. Trudnowski, J. W. Pierre, N. Zhou, J. F. Hauer, and M. Parashar, "Performance of three mode-meter block-processing algorithms for automated dynamic stability assessment," *IEEE Transactions on Power Systems*, vol. 23, no. 2, pp. 680–690, 2008.
- [62] N. E. Huang, Z. Shen, S. R. Long, M. C. Wu, H. H. Shih, Q. Zheng, N.-C. Yen, C. C. Tung, and H. H. Liu, "The empirical mode decomposition and the hilbert spectrum for nonlinear and non-stationary time series analysis," *Proceedings of the Royal Society of London. Series A: Mathematical, Physical and Engineering Sciences*, vol. 454, no. 1971, pp. 903–995, 1998.
- [63] A. R. Messina and V. Vittal, "Nonlinear, non-stationary analysis of interarea oscillations via hilbert spectral analysis," *IEEE Transactions on Power Systems*, vol. 21, no. 3, pp. 1234–1241, 2006.
- [64] T. J. Browne, V. Vittal, G. T. Heydt, and A. R. Messina, "A comparative assessment of two techniques for modal identification from power system measurements," *IEEE Transactions on Power Systems*, vol. 23, no. 3, pp. 1408–1415, 2008.
- [65] J.-N. Juang and R. S. Pappa, "An eigensystem realization algorithm for modal parameter identification and model reduction," *Journal of guidance, control, and dynamics*, vol. 8, no. 5, pp. 620–627, 1985.
- [66] E. G. Gilbert, "Controllability and observability in multivariable control systems," *Journal of the Society for Industrial and Applied Mathematics, Series A: Control*, vol. 1, no. 2, pp. 128–151, 1963.
- [67] R. E. Kalman, "Mathematical description of linear dynamical systems," *Journal of the Society for Industrial and Applied Mathematics, Series A: Control*, vol. 1, no. 2, pp. 152–192, 1963.
- [68] Y. Hua and T. K. Sarkar, "Matrix pencil method for estimating parameters of exponentially damped/undamped sinusoids in noise," *IEEE Transactions on Acoustics, Speech, and Signal Processing*, vol. 38, no. 5, pp. 814–824, 1990.
- [69] T. K. Sarkar and O. Pereira, "Using the matrix pencil method to estimate the parameters of a sum of complex exponentials," *IEEE Antennas and Propagation Magazine*, vol. 37, no. 1, pp. 48–55, 1995.

- [70] M. L. Crow and A. Singh, "The matrix pencil for power system modal extraction," *IEEE Transactions on Power Systems*, vol. 20, no. 1, pp. 501–502, 2005.
- [71] L. L. Grant and M. L. Crow, "Comparison of matrix pencil and prony methods for power system modal analysis of noisy signals," in *North American Power Symposium (NAPS), 2011*. IEEE, 2011, pp. 1–7.
- [72] Y. Hua and T. K. Sarkar, "On svd for estimating generalized eigenvalues of singular matrix pencil in noise," in *1991., IEEE International Symposium on Circuits and Systems*. IEEE, 1991, pp. 2780–2783.
- [73] T. K. Sarkar, S. Park, J. Koh, and S. M. Rao, "Application of the matrix pencil method for estimating the sem (singularity expansion method) poles of source-free transient responses from multiple look directions," *IEEE Transactions on Antennas and Propagation*, vol. 48, no. 4, pp. 612–618, 2000.
- [74] J. H. Chow, *Power system coherency and model reduction*. Springer, 2013.
- [75] S. Maslennikov, B. Wang, Q. Zhang, E. Litvinov *et al.*, "A test cases library for methods locating the sources of sustained oscillations," in *2016 IEEE Power and Energy Society General Meeting (PESGM)*. IEEE, 2016, pp. 1–5.
- [76] Test cases library of power system sustained oscillations. [Online]. Available: <http://web.eecs.utk.edu/~kaisun/Oscillation/>
- [77] E. P. T. Cari and L. F. C. Alberto, "Parameter estimation of synchronous generators from different types of disturbances," in *2011 IEEE Power and Energy Society General Meeting*. IEEE, 2011, pp. 1–7.
- [78] M. Shen, V. Venkatasubramanian, N. Abi-Samra, and D. Sobajic, "A new framework for estimation of generator dynamic parameters," *IEEE Transactions on Power Systems*, vol. 15, no. 2, pp. 756–763, 2000.
- [79] J. Sanchez-Gasca, C. Bridenbaugh, C. Bowler, and J. Edmonds, "Trajectory sensitivity based identification of synchronous generator and excitation system parameters," *IEEE Transactions on Power Systems*, vol. 3, no. 4, pp. 1814–1822, 1988.
- [80] Z. Zhao, F. Zheng, J. Gao, and L. Xu, "A dynamic on-line parameter identification and full-scale system experimental verification for large synchronous machines," *IEEE Transactions on Energy Conversion*, vol. 10, no. 3, pp. 392–398, 1995.
- [81] M. Burth, G. C. Verghese, and M. Vélez-Reyes, "Subset selection for improved parameter estimation in on-line identification of a synchronous generator," *IEEE Transactions on Power Systems*, vol. 14, no. 1, pp. 218–225, 1999.

- [82] M. Karrari and O. Malik, "Identification of physical parameters of a synchronous generator from online measurements," *IEEE transactions on energy conversion*, vol. 19, no. 2, pp. 407–415, 2004.
- [83] E. Kyriakides, G. T. Heydt, and V. Vittal, "Online parameter estimation of round rotor synchronous generators including magnetic saturation," *IEEE Transactions on Energy Conversion*, vol. 20, no. 3, pp. 529–537, 2005.
- [84] C. Lee and O. T. Tan, "A weighted-least-squares parameter estimator for synchronous machines," *IEEE Transactions on Power Apparatus and Systems*, vol. 96, no. 1, pp. 97–101, 1977.
- [85] J. R. Melgoza, G. T. Heydt, A. Keyhani, B. L. Agrawal, and D. Selin, "Synchronous machine parameter estimation using the hartley series," *IEEE transactions on energy conversion*, vol. 16, no. 1, pp. 49–54, 2001.
- [86] M. Namba, T. Nishiwaki, S. Yokokawa, and K. Ohtsuka, "Identification of parameters for power system stability analysis using kalman filter," *IEEE Transactions on Power Apparatus and Systems*, no. 7, pp. 3304–3311, 1981.
- [87] E. Eitelberg and R. Harley, "Estimating synchronous machine electrical parameters from frequency response tests," *IEEE transactions on energy conversion*, no. 1, pp. 132–138, 1987.
- [88] I. Kamwa, P. Viarouge, H. Le-Huy, and E. Dickinson, "A frequency-domain maximum likelihood estimation of synchronous machine high-order models using ssfr test data," *IEEE Transactions on Energy Conversion*, vol. 7, no. 3, pp. 525–536, 1992.
- [89] R. Escarela-Perez, T. Niewierowicz, and E. Campero-Littlewood, "Synchronous machine parameters from frequency-response finite-element simulations and genetic algorithms," *IEEE Transactions on Energy Conversion*, vol. 16, no. 2, pp. 198–203, 2001.
- [90] E. Ghahremani and I. Kamwa, "Dynamic state estimation in power system by applying the extended kalman filter with unknown inputs to phasor measurements," *IEEE Transactions on Power Systems*, vol. 26, no. 4, pp. 2556–2566, 2011.
- [91] L. Fan and Y. Wehbe, "Extended kalman filtering based real-time dynamic state and parameter estimation using pmu data," *Electric Power Systems Research*, vol. 103, pp. 168–177, 2013.
- [92] M. Ariff, B. Pal, and A. K. Singh, "Estimating dynamic model parameters for adaptive protection and control in power system," *IEEE Transactions on Power Systems*, vol. 30, no. 2, pp. 829–839, 2015.
- [93] B. Mogharbel, L. Fan, and Z. Miao, "Least squares estimation-based synchronous generator parameter estimation using pmu data," in *2015 IEEE Power & Energy Society General Meeting*. IEEE, 2015, pp. 1–5.

- [94] E. Ghahremani and I. Kamwa, "Online state estimation of a synchronous generator using unscented kalman filter from phasor measurements units," *IEEE Transactions on Energy Conversion*, vol. 26, no. 4, pp. 1099–1108, 2011.
- [95] Z. Huang, K. Schneider, and J. Nieplocha, "Feasibility studies of applying kalman filter techniques to power system dynamic state estimation," in *2007 International Power Engineering Conference (IPEC 2007)*. IEEE, 2007, pp. 376–382.
- [96] K. Kalsi, Y. Sun, Z. Huang, P. Du, R. Diao, K. K. Anderson, Y. Li, and B. Lee, "Calibrating multi-machine power system parameters with the extended kalman filter," in *2011 IEEE Power and Energy Society General Meeting*. IEEE, 2011, pp. 1–8.
- [97] Z. Huang, P. Du, D. Kosterev, and B. Yang, "Application of extended kalman filter techniques for dynamic model parameter calibration," in *2009 IEEE Power & Energy Society General Meeting*. IEEE, 2009, pp. 1–8.
- [98] J. Löfberg, "Yalmip : A toolbox for modeling and optimization in matlab," in *In Proceedings of the CACSD Conference*, Taipei, Taiwan, 2004.
- [99] A. Wächter and L. T. Biegler, "On the implementation of an interior-point filter line-search algorithm for large-scale nonlinear programming," *Mathematical programming*, vol. 106, no. 1, pp. 25–57, 2006.
- [100] L. Fan, *Control and dynamics in power systems and microgrids*. CRC Press, 2017.

Appendix A: MATLAB Code for Dynamic Parameter Estimation

```

clear;
clc;
yalmip('clear')

%Yalmip variables
H1 = sdpvar(1,1);
H2 = sdpvar(1,1);
T = sdpvar(1,1);
D1 = sdpvar(1,1);
D2 = sdpvar(1,1);
Tg1 = sdpvar(1,1);
Tg2 = sdpvar(1,1);
R1 = sdpvar(1,1);
R2 = sdpvar(1,1);

%Solver selection
ops = sdpsettings('solver','ipopt');

%From rank reduced Prony with order 5
Lambda=[ -0.31111 + 10.359i;
         -0.31111 - 10.359i;
         -5.7129e-05 + 0i;
         -0.13364 + 5.1774i;
         -0.13364 - 5.1774i;
];

e = sdpvar(length(Lambda),1,'full','complex');
w0=2*pi*60;

A=[0          w0          0          -w0          0 ;
   -T*H1/(2)  -D1*H1/(2)  H1/(2)      0          0;
   0          -Tg1*R1     -Tg1       0          0;
   T*H2/(2)   0          0          -D2*H2/(2)  H2/(2);

```



```

0          0          0          -Tg2*R2          -Tg2];

%Optimization problem constraints
for k=1:length(Lambda);
    C(k,1)=det(Lambda(k)*eye(length(Lambda))-A);
end

optimize([C == e;...
H1 >= 0; H2 >= 0; 20 >= T >= 1.6; 100 >= D1 >= 1; 100 >= D2 >= 1; Tg1 >= 0;
Tg2 >= 0; 100 >= R1 >= 1; 100 >= R2 >= 1; H1 == H2; D1 == D2], norm(e), ops)

obj = value(norm(e));



%Estimated Parameters
H1 = 1/value(H1);
H2 = 1/value(H2);
D1 = value(D1);
D2 = value(D2);
Tg1 = 1/value(Tg1);
Tg2 = 1/value(Tg2);
R1 = 1/value(R1);
R2 = 1/value(R2);
T = value(T);

```

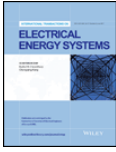
Appendix B: Copyright Permissions

- Reprint permission of published paper for Chapter 2

10/2/2019 Rightslink® by Copyright Clearance Center

Home Account Info Help LIVE CHAT



Title: Optimal PMU placement for modeling power grid observability with mathematical programming methods

Author: Lingling Fan, Anas Almunif

Publication: INTERNATIONAL TRANSACTIONS ON ELECTRICAL ENERGY SYSTEMS

Publisher: John Wiley and Sons

Date: Aug 28, 2019

© 2019 John Wiley & Sons, Ltd.

Logged in as: Anas Almunif
Account #: 3001504387
LOGOUT

Order Completed

Thank you for your order.

This Agreement between Anas Almunif ("You") and John Wiley and Sons ("John Wiley and Sons") consists of your license details and the terms and conditions provided by John Wiley and Sons and Copyright Clearance Center.

Your confirmation email will contain your order number for future reference.

[printable details](#)

License Number	4681061305789
License date	Oct 02, 2019
Licensed Content Publisher	John Wiley and Sons
Licensed Content Publication	INTERNATIONAL TRANSACTIONS ON ELECTRICAL ENERGY SYSTEMS
Licensed Content Title	Optimal PMU placement for modeling power grid observability with mathematical programming methods
Licensed Content Author	Lingling Fan, Anas Almunif
Licensed Content Date	Aug 28, 2019
Licensed Content Volume	0
Licensed Content Issue	0
Licensed Content Pages	13
Type of use	Dissertation/Thesis
Requestor type	Author of this Wiley article
Format	Print and electronic
Portion	Full article
Will you be translating?	No
Title of your thesis / dissertation	Phasor Measurement Unit Data-Based Steady State and Dynamic Model Estimation
Expected completion date	Nov 2019
Expected size (number of pages)	100
Requestor Location	Anas Almunif 4202 E Fowler Ave ENB 322 TAMPA, FL 33620

<https://s100.copyright.com/AppDispatchServlet>

1/2

- Reprint permission of Figure 1.1



October 4, 2019

Anas Almunif
Ph.D. Candidate
Department of Electrical Engineering
University of South Florida
4202 E. Fowler Ave., ENB 322
Tampa, FL 33620

Mr. Almunif,

The North American SynchroPhasor Initiative (NASPI) does not exert copyright on its publications, researchers are free to pull material from those reports and web site. NASPI grants permission, to the extent that NASPI has rights. Attribution is always appreciated. A credit line might read, "Courtesy of the North American SynchroPhasor Initiative (www.naspi.org) and the U.S. Department of Energy."

Regards,



Teresa Carlon
NASPI

- Reprint permission of Figure 1.3

10/11/2019

Web Policies | Department of Energy

receive the material, the Web address of the requested material and your first and last name, email address, and telephone number including area code.

Copyright, Restrictions and Permissions Notice

Government information at DOE websites is in the public domain. Public domain information may be freely distributed and copied, but it is requested that in any subsequent use the Department of Energy be given appropriate acknowledgement.

When using DOE websites, you may encounter documents, illustrations, photographs or other information resources contributed or licensed by private individuals, companies or organizations that may be protected by U.S. and foreign copyright laws. Transmission or reproduction of protected items beyond that allowed by fair use as defined in the copyright laws requires the written permission of the copyright owners.

Images on our website which are in the public domain may be used without permission. If you use images from our website, we ask that you credit "U.S. Department of Energy" as the source. Please note that some images on our site may have been obtained from other organizations. Permission to use these images should be obtained directly from those organizations.

DOE websites have links to many other websites. Once you access another site through a link that we provide, you are subject to the copyright and licensing restrictions of the new site.

Document Inventory and Schedule

The U.S. Department of Energy (DOE) developed this inventory of the energy.gov website content as required by Section 207(f)(2) of the E-Government Act of 2002. This inventory will be expanded and/or refined as needed depending on the information needs of our visitors.

In preparing this inventory, DOE has reviewed information collected as part of the redesign process for ENERGY.gov completed in June 2003, including citizen comments via e-mail, focus groups and usability tests; current website statistics indicating usage of existing content; and related information developed through the Information

<https://www.energy.gov/about-us/web-policies>

2/8

About the Author

Anas Almunif received the B.S. degree in electrical engineering from Taibah University, Madinah, Saudi Arabia, in 2010, and the M.S. and Ph.D. degrees in electrical engineering from University of South Florida, Tampa, FL, USA, in 2015 and 2019, respectively. Currently, he is an Assistant Professor with the Department of Electrical Engineering, Majmaah University, Majmaah, Riyadh, Saudi Arabia. His main research interests are power system monitoring and state estimation, optimization in power systems, phasor measurement unit (PMU) data identification, and system and parameter identification.